Correspondence

Biased Estimators for Spinning Antenna DOA Measurements

We propose biased estimators to find the direction of arrival of emitters present in the mainlobe of a spinning antenna-based electronic intelligence system. The proposed estimators were constructed by using Bayesian techniques and by performing a linear transformation and an affine transformation on the maximum likelihood estimator. From a Monte Carlo simulation and experimental results, we demonstrate that the proposed estimators outperform the limit set by the popular performance benchmark, the Cramér-Rao lower bound.

I. INTRODUCTION

Electronic intelligence (ELINT) is a subfield of signals intelligence, whose objective is to intercept and analyze hostile noncommunication radio frequency (RF) emissions, primarily from radars, to determine the capabilities and vulnerabilities of the adversaries [18, 46]. Extending the range at which an emitter signal can be detected and its relevant instantaneous parameters can be measured by an ELINT system is of the utmost importance. This is because an ELINT system must be able to intercept distant emitters, even if they are not aimed at friendly assets, well before the adversary can detect the ELINT system platform or site [13, 46]. This requirement was easy to achieve until emitters started to incorporate pulse compression and low probability of intercept techniques [13].

The use of a spinning high-gain directional antenna is a simple and cost-effective method of extending the detection range of an ELINT system [17]. However, the accuracy of estimating the direction of arrival (DOA) is degraded when using this antenna architecture [19] because of the partial spread of the intercepted pulses across the antenna mainlobe and the wide antenna beamwidth [22–26]. The very high pulse densities expected in the environment and the agility of the emitters' waveforms may overwhelm the ELINT system and lead to a large number of missing pulses [17, 31], which consequently result in the partial spread of the intercepted pulses across the antenna mainlobe. The wide beamwidth of the spinning antennas used in ELINT systems is necessary because of the conflicting design parameters of the spinning antenna. For example, the size of the antenna aperture needs to be constrained to

Manuscript received September 8, 2015; revised December 2, 2015; released for publication December 3, 2015.

DOI. No. 10.1109/TAES.2016.150637.

Refereeing of this contribution was handled by K. T. Wong

0018-9251/16/$26.00 © 2016 IEEE

TABLE I
Specifications of Existing Spinning Antenna (Rockwell Collins, ANT-1040A Airborne Spinning Direction-Finding Antenna) [22]

Frequency (GHz)	Beamwidth (deg)	Gain (dBi)
0.5–2	85	6.5
2	24	10.5
4	12	14.5
8	6	16.5
12	4	19
40	3	23
	Spin rates (rpm)	
	0–200	

maintain a reasonable size of the motor and to enable fast spinning so that the angular dimension is searched more quickly [16]. The small aperture size increases the antenna beamwidth, which in turn increases the speed of searching the angular dimension but reduces the antenna gain (i.e., reducing the ability to detect weak signals) [19]. A good compromise can be achieved at high frequencies. However, at low frequencies, the beam will be very wide because of the small aperture size. Table I summarizes the major parameters of an existing spinning antenna.

Although the use of a spinning (mechanical scanning) directional antenna is an old technique, it remains highly prevalent and is still used in many modern ELINT systems (see [47]). Examples of such systems are the Thales Meerkat-S ELINT system [48] and the Exelis ES-5080 ELINT system [49]. Other antenna configurations that are commonly used in ELINT systems are the phase interferometer and time difference of arrival [13, 47]. A phased array antenna might appear to be an ideal replacement for the spinning antenna, because electronic steering is conceptually appealing to eliminate mechanical motion, and it provides fast beam steering and control over the beam shape. However, there are a number of critical factors with the phased array approach. First, ELINT intercepts are not time critical; i.e., a delay in an intercept caused by the mechanical scanning of the antenna is acceptable [18, 46]. Therefore, the use of fast electronic beam steering is not critical for the success of the mission. Second, several wideband arrays are needed to achieve full azimuth coverage and to cover the required operating frequency range (0.5–40 GHz). Thus, the use of electronic beam steering is cost prohibitive and challenging to implement. Third, wideband beamforming networks (analog, digital, or optical) are required and a sufficient number of radiating elements per array are needed to achieve the desired antenna gain, which further complicates the design and raises the cost. These factors clearly indicate that mechanical scanning (spinning) suffices and that the use of electronic steering is not critical for the success of the mission. Finally, it is noteworthy that in some state-of-the-art platforms, such as the Typhoon aircraft and the F-35 aircraft, the electronic support measure (ESM) systems (ESM is somewhat related to ELINT [18, 46]) have dedicated antennas and exploit the active electronically scanned array of other systems available on the same platform (the electronic counter measure system and the radar).

To our best knowledge, no DOA estimators for spinning antenna-based ELINT systems have been reported in the literature, although spinning antenna-based DOA estimators were reported for other applications (mainly radar). In mechanically scanning radars, the two approaches to DOA estimation are the moving window (MW) approach [20] and the antenna amplitude modulation approach. The latter exploits how the mechanical scanning of the antenna impresses an amplitude modulation on the signals, which are backscattered by the target [1–7]. The MW approach exploits multiple detections at the same time on target to find the DOA [20]. The antenna amplitude modulation approach outperforms the MW approach, at the cost of more computational load [3], and is based on unbiased estimation via the maximum likelihood (ML) principle. This approach was first described by Swerling [7]. In [5, 6], approximate estimators based on this approach were proposed. Farina et al. [1, 2] extended the work on the antenna amplitude modulation approach to consider the DOA estimation of multiple targets. Then, researchers introduced high-resolution estimation methods that can resolve targets separated by less than the spinning antenna beamwidth. High-resolution DOA estimators that require multiple antenna scans to resolve targets were proposed in [27–30, 34–36], and high-resolution DOA estimators that can resolve targets using a single antenna scan were proposed in [4, 37–42]. The main drawback of the high-resolution estimators is that a full spread of the captured pulses across the antenna mainlobe and a large number of pulses and/or a high signal-to-noise ratio (SNR) are required to resolve targets. Modern ELINT systems employ digital channelization; hence, they can resolve emitters separated by less than the antenna beamwidth in the spatial domain using the emitters' frequencies [13]. Therefore, the high estimation accuracy property is more important than the high-resolution property when selecting a DOA estimator for ELINT applications.

The aforementioned estimators perform adequately with regard to the estimation accuracy (i.e., the mean square error [MSE]) for their applications. Moreover, the MSEs of some of these estimators have been shown to attain the popular performance benchmark for unbiased estimation, the Cramér-Rao lower bound (CRLB) [14]. However, we show in this work that the performance limit set by unbiased estimation bounds (i.e., the CRLB and the Barankin bound [BB]) is not adequate for the kinds of scenarios that spinning antenna-based ELINT systems might encounter, i.e., when the antenna beamwidth is wide and the number of pulses is low and/or the SNR is low or when the intercepted pulses are partially spread across the antenna mainlobe. In this work, we therefore adopt the theory of biased estimation [9–12] to obtain DOA estimators that will be better with regard to MSE and that will outperform the performance limit set by unbiased

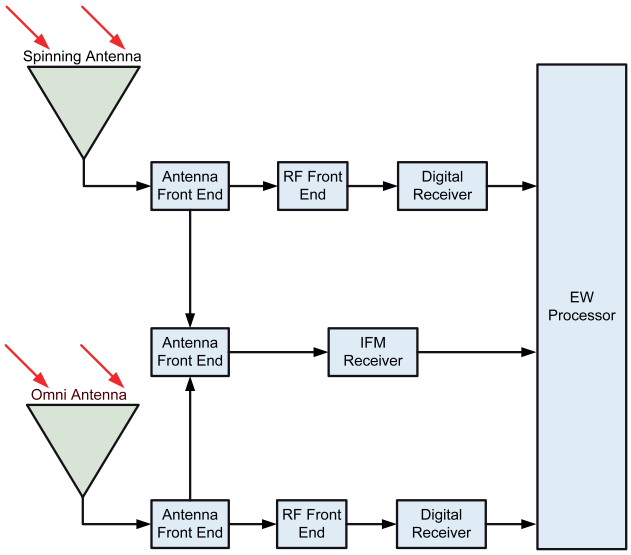

Fig. 1. Architecture of spinning antenna-based ELINT system.

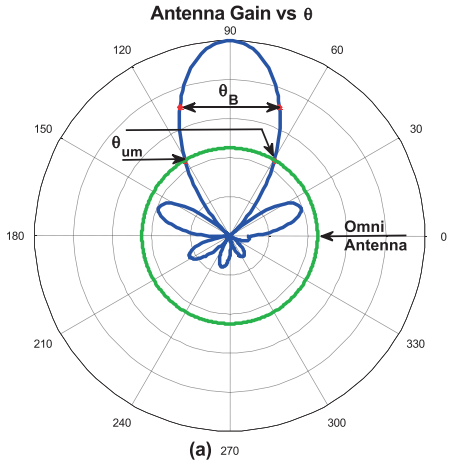

Fig. 2. Normalized antenna gain plot of two-channel spinning antenna system illustrating antenna beamwidth θ_B and unambiguous width θ_{um}.

estimation bounds. We thus present DOA estimators, which exploit how the variance of an estimator can be made smaller at the expense of increasing the bias, while ensuring that the overall MSE is reduced [8]. These proposed DOA estimators exploit the knowledge of the antenna mainlobe pattern and were constructed using the techniques described in [9–12] in conjunction with Bayesian estimation techniques [14]. We use a Monte Carlo simulation and real data to evaluate the performance of the proposed estimators and to compare the performance of the proposed estimators with estimation performance bounds.

The rest of this paper is organized as follows: The system description and the problem model are introduced in Section II. In Section III, we present the unbiased estimation performance bounds for the problem model. The ML estimator is discussed in Section IV, whereas the biased ML estimators are presented in Section V. The Bayesian estimator and the Bayesian Cramér-Rao lower bound (BCRLB) are presented in Section VI. In Section VII, the performance of the proposed estimators is evaluated by means of a Monte Carlo simulation and compared with the performance bounds. Experimental results are presented in Section VIII. Final conclusions are reported in Section IX.

II. SYSTEM DESCRIPTION AND MATHEMATICAL MODEL

Consider the ELINT system shown in Fig. 1, which consists of an instantaneous frequency measurement (IFM) receiver, a spinning high-gain antenna channel, and an omnidirectional (Omni) antenna channel; the two channels feed into digital channelized receivers. The IFM receiver provides a rapid indication of the presence of an emitter and roughly identifies the frequency of the intercepted signals so that the RF frontends feeding the digital receivers are steered into the active portion of the frequency spectrum. The Omni antenna channel provides full coverage of the field of view and measures the actual amplitude of the captured signal. In addition, the scanning patterns of the intercepted emitters are captured by the Omni antenna channel, which enables the system processor to exclude the scanning patterns from the measurements made by the spinning antenna channel so that the DOA can be estimated accurately.

As shown in Fig. 2, the relative gains of the two antenna channels are adjusted to position the Omni antenna channel gain between the spinning antenna mainlobe and its sidelobe levels [16]; thus, mainlobe detection is declared only when the spinning antenna channel output is greater than the Omni antenna channel output, which in turn must be greater than the levels of the spinning antenna sidelobes and backlobes [16]. The angular width of the mainlobe at the points where the spinning antenna channel output exceeds the Omni antenna channel output is called the unambiguous width θ_{um}.

Digital channelization is accomplished by the receiver by applying a short time Fourier transform (STFT) to the digitized signal. The STFT is equivalent to an array of adjacent finite impulse response filters [15]. If a signal presence is detected in one of the STFT parallel outputs, then the signal parameters (amplitude or complex amplitude, antenna boresight angle, frequency, modulation on pulse, time of arrival [TOA], pulse width, etc.) are measured and packed into the pulse descriptor word (PDW).

Different PDWs produced within a time frame T are grouped by the system processor based on their frequency and pulse width. The system processor estimates the DOA for each group and assigns the groups to a specific emitter based on the DOA, frequency, and pulse width. The system processor also takes into account the frequency agility of emitters; thus, it checks for groups with equal DOA and pulse width to assign those groups to the relevant emitter. This processor performs other functions too, such as

emitter tracking and identification and determination of pulse and burst repetitions intervals. ELINT systems also have the ability to digitally downconvert the intercepted signals to baseband for fine analysis and to store the signals for offline analysis [13]. More information about the architecture of modern ELINT systems and the signal processing chain is available in [15, 13, 32].

The spinning antenna, with an azimuth beamwidth θ_B, scans in the azimuth plane at angular velocity ω_R. The scanning induces amplitude modulation on the received signal; thus, the DOA can be estimated by correlating the received signal amplitude to the receiver spinning antenna pattern G. The N complex amplitudes captured by the spinning antenna mainlobe during the time on the emitter are collected in an N-dimensional column vector $\boldsymbol{Z}$; the nth component is

$$[\boldsymbol{Z}]_n = b\, G\left(\theta_{ET}, [\boldsymbol{\theta_{BO}}]_n\right) + [\boldsymbol{d}]_n; \quad n = 1, \ldots N \tag{1}$$

where $b = b_R + jb_I$ is the intercepted signal complex amplitude, modeled as a deterministic parameter, and b_R and b_I are the real and imaginary parts of the complex amplitude b. In addition, θ_{ET} is the DOA of the intercepted emitter, $\boldsymbol{d}$ is the global disturbance (thermal noise, interference, etc.), and the N-dimensional column vector $\boldsymbol{\theta_{BO}}$ is the antenna boresight angle vector. Using the following equation, $\boldsymbol{\theta_{BO}}$ relates to $\boldsymbol{TOA}$:

$$\begin{cases} [\boldsymbol{\theta_{BO}}]_n = [\boldsymbol{\theta_{BO}}]_1 + \omega_R[\boldsymbol{\Delta TOA}]_n \\ \boldsymbol{\Delta TOA} = \begin{bmatrix} 0 \\ [\boldsymbol{TOA}]_2 - [\boldsymbol{TOA}]_1 \\ \vdots \\ \vdots \\ [\boldsymbol{TOA}]_n - [\boldsymbol{TOA}]_1 \end{bmatrix} \end{cases} \tag{2}$$

The vector notation of (1) is given by the following:

$$\boldsymbol{Z} = \boldsymbol{S} + \boldsymbol{d} = b\boldsymbol{a}\left(\theta_{ET}, \boldsymbol{\theta_{BO}}\right) + \boldsymbol{d} \tag{3}$$

The N-dimensional disturbance complex vector $\boldsymbol{d}$ has a Gaussian probability density function (pdf) with zero mean and a known $N \times N$-dimensional covariance matrix $\boldsymbol{R} = E\{\boldsymbol{dd^H}\} = \sigma_d^2 \boldsymbol{M}$, where $(\,)^{\mathbf{H}}$ is the conjugate-transpose operator, σ_d^2 is the total disturbance power, and $\boldsymbol{M}$ is the normalized covariance matrix. In this work, we assume that the disturbance consists of complex zero-mean white Gaussian noise that has a covariance matrix $\boldsymbol{R} = \sigma_d^2 \boldsymbol{I}$, where $\boldsymbol{I}$ is the identity matrix. The nth component of the N-dimensional emitter steering vector $\boldsymbol{a}(\theta_{ET}, \boldsymbol{\theta_{BO}})$ is as follows:

$$[\boldsymbol{a}\left(\theta_{ET}, \boldsymbol{\theta_{BO}}\right)]_n = G\left(\theta_{ET}, [\boldsymbol{\theta_{BO}}]_n\right); \quad n = 1, \ldots N \tag{4}$$

Finally, the pdf of $\boldsymbol{Z}$ conditioned to b and θ_{ET} is as follows:

$$P_{\boldsymbol{Z}/\boldsymbol{S}}(\boldsymbol{Z}; b, \theta_{ET}) = \frac{1}{\pi^N \det(\boldsymbol{R})} \exp\left[-[\boldsymbol{Z} - \boldsymbol{a}(\theta_{ET}, \boldsymbol{\theta_{BO}})b]^H \times \boldsymbol{R}^{-1}\left[\boldsymbol{Z} - \boldsymbol{a}\left(\theta_{ET}, \boldsymbol{\theta_{BO}}\right) b\right]\right] \tag{5}$$

The aforementioned problem formulation is similar to that derived by Farina et al. in [1, 2], when they studied the estimation of radar targets' DOA by using the ML estimator.

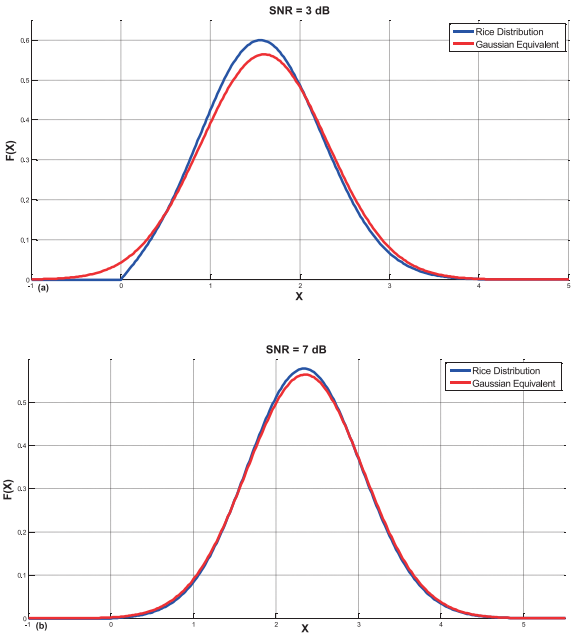

Fig. 3. Plots of Rician distribution versus equivalent Gaussian distribution at different SNR values. (a) SNR = 3 dB. (b) SNR = 7 dB.

Modern ELINT systems can digitally downconvert the intercepted signals to baseband [13], which in principle implies that the complex amplitude can be measured. However, measuring the intercepted signal's complex amplitude can be challenging because of the uncertainty of the intercepted signal's modulation scheme and errors in estimating the carrier frequency. It is common for practical ELINT systems to measure the amplitude $[\boldsymbol{\zeta}]_n = (\mathrm{Re}\{[\boldsymbol{Z}]_n\}^2 + \mathrm{Im}\{[\boldsymbol{Z}]_n\}^2)^{\frac{1}{2}}$ of the intercepted signal rather than the complex amplitude $[\boldsymbol{Z}]_n$ [13, 15, 17, 19, 32]. Therefore, DOA estimation using the intercepted signal amplitude when the Gaussian disturbance $\boldsymbol{d}$ is statistically independent (i.e., white Gaussian noise) is investigated. The amplitude $[\boldsymbol{\zeta}]_n$ of the nth component of the N-dimensional complex amplitude vector $\boldsymbol{Z} \in \mathcal{CN}(b\boldsymbol{a}(\theta_{ET}, \boldsymbol{\theta_{BO}}), \boldsymbol{R})$ is Rician distributed:

$$P_{[\boldsymbol{\zeta}]_n/[\boldsymbol{Z}]_n}\left([\boldsymbol{\zeta}]_n; \beta, \theta_{ET}\right) = \frac{2[\boldsymbol{\zeta}]_n}{\sigma_d^2} \exp\left[\frac{-\left([\boldsymbol{\zeta}]_n^2 + \beta^2\left[\boldsymbol{a}\left(\theta_{ET}, \boldsymbol{\theta_{BO}}\right)\right]_n^2\right)}{\sigma_d^2}\right] \times I_0\left(\frac{2[\boldsymbol{\zeta}]_n \beta[\boldsymbol{a}\left(\theta_{ET}, \boldsymbol{\theta_{BO}}\right)]_n}{\sigma_d^2}\right) \tag{6}$$

where I_0 is the modified zeroth-order Bessel function of the first kind and $\beta = (b_R^2 + b_I^2)^{\frac{1}{2}}$ is the magnitude of the complex amplitude b. Re{ } and Im{ } are the real and the imaginary of the complex quantity, respectively. The dependency of $\boldsymbol{a}(\theta_{ET}, \boldsymbol{\theta_{BO}})$ on θ_{ET} and $\boldsymbol{\theta_{BO}}$ was omitted from the following sections for ease of notation.

As shown in Fig. 3, the Rician distribution can be approximated to a Gaussian distribution to simplify the

derivation of estimators. This is because the Rician distribution of $\boldsymbol{\zeta}$ is equivalent to the Rayleigh distribution when there is no signal and is approximately Gaussian with mean $\boldsymbol{m}_{\boldsymbol{\zeta}} \cong (\boldsymbol{a} \odot \boldsymbol{a}\beta^2 + \frac{\sigma_d^2}{2})^{\odot \frac{1}{2}}$ at moderate to high SNR, where at very high SNR the mean becomes $\boldsymbol{m}_{\boldsymbol{\zeta}} \cong \beta \boldsymbol{a}$. This equivalent Gaussian distribution has a covariance matrix $\boldsymbol{C} = \frac{\sigma_d^2}{2}\boldsymbol{I}$ and a pdf given by the following expression:

$$P_{\boldsymbol{\zeta}/\boldsymbol{Z}}(\boldsymbol{\zeta}; \beta, \theta_{ET}) = \frac{1}{\sqrt{2\pi^N \det(\boldsymbol{C})}} \exp\left[-\frac{1}{2}\left[\boldsymbol{\zeta} - \left(\boldsymbol{a} \odot \boldsymbol{a}\beta^2 + \frac{\sigma_d^2}{2}\right)^{\odot \frac{1}{2}}\right]^T \times \boldsymbol{C}^{-1}\left[\boldsymbol{\zeta} - \left(\boldsymbol{a} \odot \boldsymbol{a}\beta^2 + \frac{\sigma_d^2}{2}\right)^{\odot \frac{1}{2}}\right]\right] \quad (7)$$

where $\odot$ is the Hadamard product or element-wise multiplication [33], $(\,)^{\boldsymbol{T}}$ is the transpose operator, and $\boldsymbol{\zeta}$ is the N-dimensional captured amplitudes column vector. Similar approximations to the Rician distribution were reported by Lie et al. [29].

III. PERFORMANCE BOUNDS FOR UNBIASED ESTIMATION

A. The CRLB

The CRLB is presented here to determine the performance limit that could be achieved for the possible scenarios that spinning antenna-based ELINT systems might encounter. Moreover, the CRLB is used to calculate the transformation parameters of the proposed biased ML estimators.

1) *Complex Amplitude Case*: The data vector $\boldsymbol{Z}$ is complex Gaussian distributed, with mean $\boldsymbol{m}_{\boldsymbol{Z}} = E\{\boldsymbol{Z}\} = (b_R + jb_I)\,\boldsymbol{a}$ and covariance matrix $\boldsymbol{R}$. The 3×1 unknown parameter vector is $\boldsymbol{\vartheta} = [\theta_{ET} \;\; b_R \;\; b_I]^T$. The elements of the 3×3 Fisher information matrix are obtained as

$$[\boldsymbol{J}]_{ij} = 2\mathrm{Re}\left\{\frac{\partial \boldsymbol{m}_{\boldsymbol{Z}}^H}{\partial[\boldsymbol{\vartheta}]_i}\boldsymbol{R}^{-1}\frac{\partial \boldsymbol{m}_{\boldsymbol{Z}}}{\partial[\boldsymbol{\vartheta}]_j}\right\}; \quad i, j = 1, 2, 3 \quad (8)$$

$$\frac{\partial \boldsymbol{m}_{\boldsymbol{Z}}}{\partial[\boldsymbol{\vartheta}]_i} = \begin{cases} (b_R + jb_I)\,\boldsymbol{a}_{\boldsymbol{\theta}} \\ \boldsymbol{a} \\ j\,\boldsymbol{a} \end{cases} \quad (9)$$

where $\boldsymbol{a}_{\boldsymbol{\theta}}$ is the gradient, with respect to θ_{ET}, of the vector $\boldsymbol{a}$.

2) *Amplitude Case*: The data vector $\boldsymbol{\zeta}$ is modeled as real Gaussian distributed with mean $\boldsymbol{m}_{\boldsymbol{\zeta}} = E\{\boldsymbol{\zeta}\} \cong (\boldsymbol{a} \odot \boldsymbol{a}\beta^2 + \frac{\sigma_d^2}{2})^{\odot \frac{1}{2}}$ and covariance matrix $\boldsymbol{C}$. The 2×1 unknown parameter vector is $\boldsymbol{\vartheta} = [\theta_{ET} \;\; \beta]^T$. The elements of the 2×2 Fisher information matrix are obtained as follows:

$$[\boldsymbol{J}]_{ij} = \left\{\frac{\partial \boldsymbol{m}_{\boldsymbol{\zeta}}^T}{\partial[\boldsymbol{\vartheta}]_i}\boldsymbol{C}^{-1}\frac{\partial \boldsymbol{m}_{\boldsymbol{\zeta}}}{\partial[\boldsymbol{\vartheta}]_j}\right\}; \quad i, j = 1, 2 \quad (10)$$

TABLE II
Simulation Setups Used to Plot CRLB Curves with Different Parameters[1]

CRLB	$\theta_B = \theta_{um}$	θ_{ET}	N	$PRI\omega_R$	$[\boldsymbol{\theta_{BO}}]_1$	$[\boldsymbol{\theta_{BO}}]_N$
1	30°	15°	16	1.875°	0°	28.125°
2	30°	15°	8	3.75°	0°	26.25°
3	10°	5°	16	0.625°	0°	9.375°
4	10°	5°	8	1.25°	0°	8.75°

Parameters listed are spinning antenna beamwidth θ_B, unambiguous width θ_{um}, emitter DOA θ_{ET}, number of pulses N, the product of the pulse repetition interval and angular velocity ($PRI\omega_R$), and antenna boresight angle vector $\boldsymbol{\theta_{BO}}$.

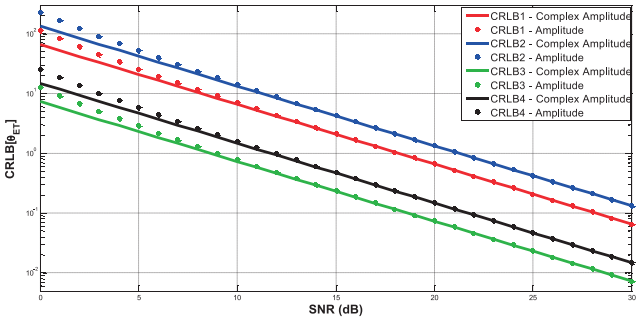

Fig. 4. Plots of $CRLB\{\hat{\theta}_{ET}\}$ with different parameters, as given in Table II.

$$\frac{\partial \boldsymbol{m}_{\boldsymbol{\zeta}}}{\partial[\boldsymbol{\vartheta}]_i} = \begin{cases} \beta^2\,\boldsymbol{a} \odot \boldsymbol{a}_{\theta} \odot \left(\boldsymbol{a} \odot \boldsymbol{a}\beta^2 + \frac{\sigma_d^2}{2}\right)^{\odot \frac{-1}{2}} \\ \beta\,\boldsymbol{a} \odot \boldsymbol{a} \odot \left(\boldsymbol{a} \odot \boldsymbol{a}\beta^2 + \frac{\sigma_d^2}{2}\right)^{\odot \frac{-1}{2}} \end{cases} \quad (11)$$

The CRLBs are given by the diagonal elements of $\boldsymbol{J}^{-1}$, i.e., $CRLB([\boldsymbol{\vartheta}]_i) = [\boldsymbol{J}^{-1}]_{ii}$.

Plots of the CRLB for both cases, with different parameter values as listed in Table II, are shown in Fig. 4. The results obtained clearly show that the CRLB is poor when the antenna beamwidth is wide and the number of pulses is low and/or the SNR is low. The accuracy of estimating the DOA can be improved by increasing the bias to reduce the variance while ensuring that the overall MSE is minimized. This can be achieved by either using Bayesian estimators or introducing a bias to the unbiased estimator.

B. The BB

Any unbiased estimator exhibits the threshold effect, in which the MSE performance of the unbiased estimator deviates substantially from the CRLB below a certain SNR; thus, the use of the CRLB to predict the performance of the estimator below the threshold point is not valid [44]. The BB is significantly tighter than the CRLB at low SNR values [44], and is presented here to determine the SNR threshold point. The BB on the MSE of any unbiased estimator of $\boldsymbol{\vartheta}$ is given by the diagonal elements of the matrix $\boldsymbol{\Lambda}$; i.e., $BB(\boldsymbol{\vartheta}_i) = [\boldsymbol{\Lambda}]_{ii}$. Here, $\boldsymbol{\Lambda}$ is [44]

$$\boldsymbol{\Lambda} = \boldsymbol{T}\left(\boldsymbol{D} - \boldsymbol{1}\boldsymbol{1}^T\right)^{-1}\boldsymbol{T}^T \quad (12)$$

TABLE III
Simulation Setups Used to Plot BB Curves with Different Parameters[1]

Setup	$\theta_B = \theta_{um}$	θ_{ET}	N	$PRI\omega_R$	$[\boldsymbol{\theta_{BO}}]_1$	$[\boldsymbol{\theta_{BO}}]_N$
1	30°	15°	4	7.5°	0°	22.5°
2	30°	15°	32	0.9375°	0°	29.0625°

Parameters listed are spinning antenna beamwidth θ_B, unambiguous width θ_{um}, emitter DOA θ_{ET}, number of pulses N, the product of the pulse repetition interval and angular velocity ($PRI\omega_R$), and antenna boresight angle vector $\boldsymbol{\theta_{BO}}$.

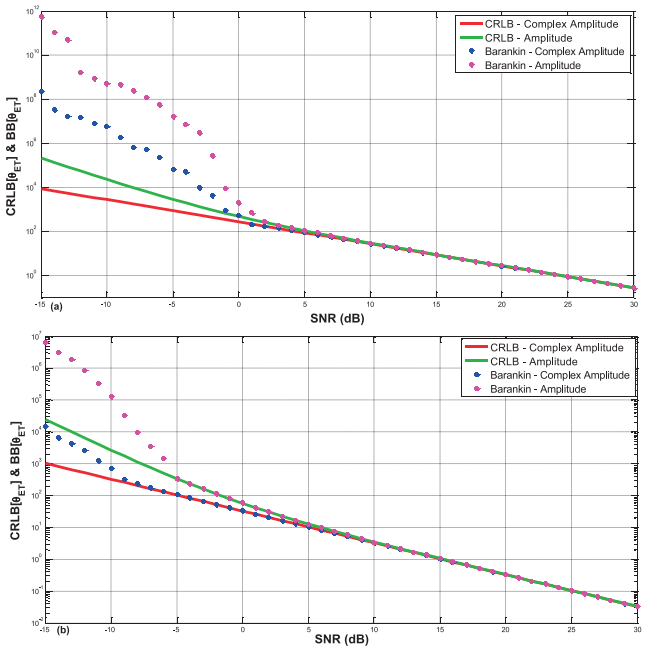

Fig. 5. Plots of $CRLB\{\hat{\theta}_{ET}\}$ and $BB\{\hat{\theta}_{ET}\}$ with different parameters, as given in Table III. (a) Setup 1. (b) Setup 2.

and the matrix $\boldsymbol{T}$ is defined as

$$\boldsymbol{T} = \left[\boldsymbol{\vartheta}_1 - \boldsymbol{\vartheta}, \boldsymbol{\vartheta}_2 - \boldsymbol{\vartheta}, \ldots \boldsymbol{\vartheta}_p - \boldsymbol{\vartheta}\right] \tag{13}$$

where $\boldsymbol{\vartheta}_i, i = 1 \ldots p$ are called test points and chosen to maximize the right-hand side of (12). The vector $\mathbf{1}$ is of size P whose elements are equal to 1. The elements of the Barankin matrix $\boldsymbol{D}$ are given as follows [45].

1) *Complex Amplitude Case*:

$$[\boldsymbol{D}(\boldsymbol{\vartheta})]_{ij} = \exp\left[2\mathrm{Re}\left\{(\boldsymbol{m_Z}(\boldsymbol{\vartheta}) - \boldsymbol{m_Z}(\boldsymbol{\vartheta}_i))^H \boldsymbol{R}^{-1}(\boldsymbol{m_Z}(\boldsymbol{\vartheta}) - \boldsymbol{m_Z}(\boldsymbol{\vartheta}_j))\right\}\right]; \quad i, j = 1, 2, \ldots p \tag{14}$$

2) *Amplitude Case*:

$$[\boldsymbol{D}(\boldsymbol{\vartheta})]_{ij} = \exp\left[\left(\boldsymbol{m_\zeta}(\boldsymbol{\vartheta}) - \boldsymbol{m_\zeta}(\boldsymbol{\vartheta}_i)\right)^T \boldsymbol{C}^{-1}\left(\boldsymbol{m_\zeta}(\boldsymbol{\vartheta}) - \boldsymbol{m_\zeta}(\boldsymbol{\vartheta}_j)\right)\right]; \quad i, j = 1, 2, \ldots p \tag{15}$$

Plots of the BB with different parameter values, as listed in Table III, are shown in Fig. 5. Results in Fig. 5 show that the threshold effect occurs at a very small SNR value, even when the number of pulses is low.

IV. THE ML ESTIMATOR

The ML estimator is an unbiased classical estimator in which the parameter of interest (DOA) is assumed to be deterministic but unknown.

1) *Complex Amplitude Case*: The ML estimator is obtained by maximizing the pdf given in (5) with respect to the deterministic parameters b and θ_{ET}. The ML estimator is given by the following expressions [1, 2]:

$$\begin{cases} \hat{b} = \dfrac{\boldsymbol{a}^H \boldsymbol{R}^{-1} \boldsymbol{Z}}{\boldsymbol{a}^H \boldsymbol{R}^{-1} \boldsymbol{a}} \\ \hat{\theta}_{ET} = \arg\max\limits_{\theta_{ET}} \dfrac{\left|\boldsymbol{Z}^H \boldsymbol{R}^{-1} \boldsymbol{a}\right|^2}{\boldsymbol{a}^H \boldsymbol{R}^{-1} \boldsymbol{a}} \end{cases} \tag{16}$$

2) *Amplitude Case*: The ML estimator is obtained by maximizing the log-likelihood of (6) with respect to the deterministic parameters β and θ_{ET}. After some simplification, the ML estimator is given by the following expression:

$$\left(\hat{\theta}_{ET}, \hat{\beta}\right) = \arg\max_{\beta, \theta_{ET}} \sum_{n=1}^{N} \left(\log I_0\left(\frac{2[\boldsymbol{\zeta}]_n \beta [\boldsymbol{a}]_n}{\sigma_d^2}\right) - \frac{\beta^2 [\boldsymbol{a}]_n^2}{\sigma_d^2}\right) \tag{17}$$

This estimator requires the solution of two-dimensional (2D) nonlinear maximization and the computation of the Bessel function. A simpler estimator can be found using the equivalent Gaussian pdf given in (7). The ML estimator for the approximated model is obtained by maximizing the pdf given in (7). After some simplification, the ML estimator is given by the following expression:

$$\left(\hat{\theta}_{ET}, \hat{\beta}\right) = \arg\max_{\beta, \theta_{ET}} \left[2\boldsymbol{\zeta}^T \left(\boldsymbol{a} \odot \boldsymbol{a}\beta^2 + \frac{\sigma_d^2}{2}\right)^{\odot \frac{1}{2}}\right] - \left[\left(\boldsymbol{a} \odot \boldsymbol{a}\beta^2 + \frac{\sigma_d^2}{2}\right)^{\odot \frac{1}{2}}\right]^T \left[\left(\boldsymbol{a} \odot \boldsymbol{a}\beta^2 + \frac{\sigma_d^2}{2}\right)^{\odot \frac{1}{2}}\right] \tag{18}$$

This estimator also requires the solution of 2D nonlinear maximization, but it is easier to implement than the 2D Rician ML. The complexity can be reduced by using a suboptimal estimator for β to reduce the estimator to a one-dimensional problem. The mean equals $\boldsymbol{m_\zeta} \cong \beta \boldsymbol{a}$ at a high SNR, and then the equivalent Gaussian pdf becomes as follows:

$$P_{\zeta/Z}(\boldsymbol{\zeta}; \beta, \theta_{ET}) = \frac{1}{\sqrt{2\pi^N \det(\boldsymbol{C})}} \exp\left[-\frac{1}{2}[\boldsymbol{\zeta} - \beta \boldsymbol{a}]^T \boldsymbol{C}^{-1} [\boldsymbol{\zeta} - \beta \boldsymbol{a}]\right] \tag{19}$$

Then, the suboptimal estimator for β is found by maximizing the pdf given in (19) with respect to β. After some simplification, the estimator for β is given by the following:

$$\hat{\beta} = \frac{\boldsymbol{a}^T \boldsymbol{\zeta}}{\boldsymbol{a}^T \boldsymbol{a}} \tag{20}$$

Finally, the ML estimator for θ_{ET} is given by the following expression:

$$\hat{\theta}_{ET} = \arg\max_{\theta_{ET}} \left[2\boldsymbol{\zeta}^T \left(\boldsymbol{a} \odot \boldsymbol{a} \left| \frac{\boldsymbol{a}^T \boldsymbol{\zeta}}{\boldsymbol{a}^T \boldsymbol{a}} \right|^2 + \frac{\sigma_d^2}{2} \right)^{\odot \frac{1}{2}} \right] - \left[\left(\boldsymbol{a} \odot \boldsymbol{a} \left| \frac{\boldsymbol{a}^T \boldsymbol{\zeta}}{\boldsymbol{a}^T \boldsymbol{a}} \right|^2 + \frac{\sigma_d^2}{2} \right)^{\odot \frac{1}{2}} \right]^T \left[\left(\boldsymbol{a} \odot \boldsymbol{a} \left| \frac{\boldsymbol{a}^T \boldsymbol{\zeta}}{\boldsymbol{a}^T \boldsymbol{a}} \right|^2 + \frac{\sigma_d^2}{2} \right)^{\odot \frac{1}{2}} \right] \tag{21}$$

V. BIASED ML ESTIMATORS

A. Linear Bias

The performance of an unbiased estimator (the ML estimator) can be improved by introducing a linear bias [10]. The linearly transformed ML estimator is given by [10]

$$\hat{\theta}_b = (1+m)\,\hat{\theta}_u \tag{22}$$

where $\hat{\theta}_u$ is the unbiased estimator (ML estimator) and m ($-1 \leq m < 0$) is a transformation parameter, which introduces a bias to the unbiased estimator. The MSE for the biased estimator $\hat{\theta}_b$ is given by [10]

$$MSE\left(\hat{\theta}_b\right) = (1+m)^2 var\left(\hat{\theta}_u\right) + m^2\theta^2 \tag{23}$$

where $var(\,)$ is the variance of an estimator. The value of m that minimizes the overall MSE, trading an increase in bias for a decrease in variance, is found by solving the following minimax equation [10]:

$$m = \arg\min_m \max_\theta \left\{ MSE\left(\hat{\theta}_b\right) - MSE\left(\hat{\theta}_u\right) \right\} \tag{24}$$

Here, θ lies in the following interval:

$$[\boldsymbol{\theta_{BO}}]_N - \frac{\theta_{um}}{2} \leq \theta \leq [\boldsymbol{\theta_{BO}}]_1 + \frac{\theta_{um}}{2} \tag{25}$$

The interval specified by (25) can be written as quadratic constraint Q [10]:

$$Q = \left\{ \theta : \theta^T A_1 \theta + 2\, b_1 \theta + c_1 \leq 0 \right\} \tag{26}$$

In our case, the values of A_1, b_1, and c_1 are as follows:

$$\begin{cases} A_1 = 1 \\ b_1 = -\dfrac{[\boldsymbol{\theta_{BO}}]_N + [\boldsymbol{\theta_{BO}}]_1}{2} \\ c_1 = \left([\boldsymbol{\theta_{BO}}]_N - \dfrac{\theta_{um}}{2} \right) \left([\boldsymbol{\theta_{BO}}]_1 + \dfrac{\theta_{um}}{2} \right) \end{cases} \tag{27}$$

The procedure described in [10] is followed to solve (24); the first step is to curve fit the CRLB to the following quadratic form [10]:

$$CRLB\,(\theta) = B_1 \theta \theta^T B_1^T + \left(C_1 \theta z_1^T + z_1 \theta^T C_1^T \right) + A \tag{28}$$

The optimal value of m is given by the following equation [10]:

$$m = -S\,(\Pi, w)\,(S\,(\Pi, w) + \Pi)^{-1} \tag{29}$$

Here, $S(\Pi, w)$ is given by [10]

$$S\,(\Pi, w) = B_1 \Pi B_1^T + \left(C_1 w^T z_1^T + z_1 w\, C_1^T \right) + A \tag{30}$$

where Π and w are the solutions to the following semidefinite programming problem (SDP) [10]:

$$\begin{cases} \min\limits_{Y,w,\Pi} Tr\,(Y) \\ s.t. \begin{bmatrix} Y & S\,(\Pi, w) \\ S\,(\Pi, w) & S\,(\Pi, w) + \Pi \end{bmatrix} \geq 0 \\ \begin{bmatrix} \Pi & w \\ w & 1 \end{bmatrix} \geq 0 \\ \Pi A_1 + 2wb_1 + c_1 \leq 0 \end{cases} \tag{31}$$

The OPTI Toolbox [21] was used to solve (31).

In the case of a constant CRLB [10],

$$m = -\frac{CRLB}{CRLB\ +\ V^2} \tag{32}$$

where V is the upper limit of the interval specifying θ.

B. Affine Bias

The MSE can be further reduced by introducing an affine bias of the form [11]

$$\hat{\theta}_b = (1+m)\,\hat{\theta}_u + u \tag{33}$$

where m and u are transformation parameters that introduce a bias to the unbiased estimator $\hat{\theta}_u$ (the ML estimator). The MSE for the biased estimator $\hat{\theta}_b$ is given by the following [11]:

$$MSE\left(\hat{\theta}_b\right) = (1+m)^2 var\left(\hat{\theta}_u\right) + (m\theta + u)^2 \tag{34}$$

The values of m and u that minimize the overall MSE, trading an increase in bias for a decrease in variance, are found by solving the following minimax equation [11]:

$$(m, u) = \arg\min_{m,u} \max_\theta \left\{ MSE\left(\hat{\theta}_b\right) - MSE\left(\hat{\theta}_u\right) \right\} \tag{35}$$

The interval, where θ lies, is defined in (25).

The procedure described in [11] is followed to solve (35); the first step is to curve fit the CRLB to the quadratic form specified by (28) [11]. The optimal values of m and u are given by the following equations [11]:

$$m = -S\,(\Pi, w)\left(S\,(\Pi, w) + \Pi - ww^T \right)^{-1} \tag{36}$$

$$u = \frac{1}{1 - w^T (S\,(\Pi, w) + \Pi)^{-1} w} S\,(\Pi, w) \times (S\,(\Pi, w) + \Pi)^{-1}\, w \tag{37}$$

Here, $S(\Pi, w)$ is given by [11]

$$S\,(\Pi, w) = B_1 \Pi B_1^T + \left(C_1 w z_1^T + z_1 w C_1^T \right) + A \tag{38}$$

where Π and w are the solutions to the following SDP [11]:

$$\begin{cases} \min\limits_{Y,w,\Pi} Tr\,(Y) \\ s.t. \begin{bmatrix} Y & S(\Pi,w) & 0 \\ S(\Pi,w) & S(\Pi,w)+\Pi & w \\ 0 & w & 1 \end{bmatrix} \geq 0 \\ \begin{bmatrix} \Pi & w \\ w & 1 \end{bmatrix} \geq 0 \\ \Pi A_1 + 2wb_1 + c_1 \leq 0 \end{cases} \tag{39}$$

The OPTI Toolbox [21] was used to solve (39).

In case of a constant CRLB, m and u as follows [11]:

$$m = -\frac{CRLB}{CRLB + b_1^T b_1 - c_1} \tag{40}$$

$$u = -\frac{CRLB}{CRLB + b_1^T b_1 - c_1} b_1 \tag{41}$$

VI. THE BAYESIAN ESTIMATOR

In the Bayesian estimation of deterministic parameters, the deterministic parameters are treated as if they were random, but the randomness is only introduced through observations and prior distributions are adopted to impose certain constraints [43]. A Bayesian estimator for a deterministic parameter trades bias for variance in an attempt to reduce the overall MSE; thus, it outperforms the efficient unbiased estimator (i.e., the unbiased estimator that attains the CRLB) on average, but it may perform poorly for certain values of the unknown parameter [14, 43]. Such poor performance is because of the substantial increase in the bias, which can be avoided by accurately setting the prior pdf parameters so that proper bias is introduced, thereby ensuring improved performance [14, 43]. In this work, we have used the minimum mean square error (MMSE) estimator to estimate the DOA.

A. The MMSE Estimator

The MMSE estimator is a popular form of Bayesian estimation techniques. The closed form of this estimator can be found if both the measurement and the prior pdfs are Gaussian [14]. This closed form is given by

$$E(\boldsymbol{\vartheta}|\boldsymbol{X}) = \boldsymbol{\mu} + \boldsymbol{\Gamma}\boldsymbol{H}^H\left(\boldsymbol{H}\boldsymbol{\Gamma}\boldsymbol{H}^H + \boldsymbol{\Sigma}\right)^{-1}(\boldsymbol{X} - \boldsymbol{H}\boldsymbol{\mu}) \tag{42}$$

where $\boldsymbol{X}$ is an $N \times 1$ data vector, $\boldsymbol{H}$ is a known $N \times K$ matrix, $\boldsymbol{\vartheta}$ is a $K \times 1$ unknown vector with prior pdf $\mathcal{N}(\boldsymbol{\mu}, \boldsymbol{\Gamma})$, and $\boldsymbol{d}$ is an $N \times 1$ noise vector with pdf $C\mathcal{N}(0, \boldsymbol{\Sigma})$.

1) *Complex Amplitude Case*: Using local linearization approximation around the prior mean, (5) and (42), the MMSE estimator of the 3×1 parameter vector $\boldsymbol{\vartheta} = [\theta_{ET}\ b_R\ \ b_I]^T$ is

$$\hat{\boldsymbol{\vartheta}} = \mathrm{Re}\left\{\boldsymbol{\mu} + \boldsymbol{\Gamma}\boldsymbol{H}^H\left(\mathbf{H}\boldsymbol{\Gamma}\boldsymbol{H}^{\mathbf{H}} + \mathbf{R}\right)^{-1}(\boldsymbol{Z} - \mathbf{m}_{\boldsymbol{Z}}(\boldsymbol{\mu}))\right\} \tag{43}$$

where $\boldsymbol{\mu}$ is the prior mean $\boldsymbol{\mu} = [\theta_\mu\ \ b_{\mu R}\ \ b_{\mu I}]^T$. The columns of the matrix $\boldsymbol{H}$ and the diagonal elements of the diagonal matrix $\boldsymbol{\Gamma}$ are given by the following:

$$\begin{cases} [\boldsymbol{H}]_{:1} = \left(b_{\mu R} + jb_{\mu I}\right)\boldsymbol{a}_{\boldsymbol{\theta}}\left(\theta_\mu, \boldsymbol{\theta}_{\boldsymbol{BO}}\right) \\ [\boldsymbol{H}]_{:2} = \boldsymbol{a}\left(\theta_\mu, \boldsymbol{\theta}_{\boldsymbol{BO}}\right) \\ [\boldsymbol{H}]_{:3} = j\boldsymbol{a}\left(\theta_\mu, \boldsymbol{\theta}_{\boldsymbol{BO}}\right) \\ [\boldsymbol{\Gamma}]_{11} = v^2 \\ [\boldsymbol{\Gamma}]_{22} = \left(b_{\mu R} - b_{vR}\right)^2 \\ [\boldsymbol{\Gamma}]_{33} = \left(b_{\mu I} - b_{vI}\right)^2 \end{cases} \tag{44}$$

We found through a Monte Carlo simulation that the values of the prior Gaussian pdf parameters that result in the best estimate of θ_{ET} are obtained as

$$\begin{cases} \theta_\mu = [\boldsymbol{\theta}_{\boldsymbol{BO}}]_1 + \dfrac{[\boldsymbol{\theta}_{\boldsymbol{BO}}]_N - [\boldsymbol{\theta}_{\boldsymbol{BO}}]_1}{2} \\ v = \dfrac{1}{2}\left(\theta_{um} - \left([\boldsymbol{\theta}_{\boldsymbol{BO}}]_N - [\boldsymbol{\theta}_{\boldsymbol{BO}}]_1\right)\right) \\ b_{\mu R} = \mathrm{Re}\left\{\dfrac{\boldsymbol{a}\left(\theta_\mu, \boldsymbol{\theta}_{\boldsymbol{BO}}\right)^H \boldsymbol{R}^{-1}\boldsymbol{Z}}{\boldsymbol{a}\left(\theta_\mu, \boldsymbol{\theta}_{\boldsymbol{BO}}\right)^H \boldsymbol{R}^{-1}\boldsymbol{a}\left(\theta_\mu, \boldsymbol{\theta}_{\boldsymbol{BO}}\right)}\right\} \\ b_{\mu I} = \mathrm{Im}\left\{\dfrac{\boldsymbol{a}\left(\theta_\mu, \boldsymbol{\theta}_{\boldsymbol{BO}}\right)^H \boldsymbol{R}^{-1}\boldsymbol{Z}}{\boldsymbol{a}\left(\theta_\mu, \boldsymbol{\theta}_{\boldsymbol{BO}}\right)^H \boldsymbol{R}^{-1}\boldsymbol{a}\left(\theta_\mu, \boldsymbol{\theta}_{\boldsymbol{BO}}\right)}\right\} \\ b_{vR} = \mathrm{Re}\left\{\dfrac{\boldsymbol{a}\left(\theta_\mu + v, \boldsymbol{\theta}_{\boldsymbol{BO}}\right)^H \boldsymbol{R}^{-1}\boldsymbol{Z}}{\boldsymbol{a}\left(\theta_\mu + v, \boldsymbol{\theta}_{\boldsymbol{BO}}\right)^H \boldsymbol{R}^{-1}\boldsymbol{a}\left(\theta_\mu + v, \boldsymbol{\theta}_{\boldsymbol{BO}}\right)}\right\} \\ b_{vI} = \mathrm{Im}\left\{\dfrac{\boldsymbol{a}\left(\theta_\mu + v, \boldsymbol{\theta}_{\boldsymbol{BO}}\right)^H \boldsymbol{R}^{-1}\boldsymbol{Z}}{\boldsymbol{a}\left(\theta_\mu + v, \boldsymbol{\theta}_{\boldsymbol{BO}}\right)^H \boldsymbol{R}^{-1}\boldsymbol{a}\left(\theta_\mu + v, \boldsymbol{\theta}_{\boldsymbol{BO}}\right)}\right\} \end{cases} \tag{45}$$

where θ_μ is the average of the angle of the antenna boresight at the first intercepted pulse and the angle of the antenna boresight at the last intercepted pulse, v is the unambiguous width minus the span of the intercepted pulses across the unambiguous width, and $b_{\mu R}$, $b_{\mu I}$, b_{vR}, and b_{vI} are the complex amplitude parts that are calculated at angles θ_μ and $\theta_\mu + v$.

2) *Amplitude Case*: Following the same procedure used for the complex amplitude case, the MMSE estimator of the 2×1 parameter vector $\boldsymbol{\vartheta} = [\theta_{ET}\ \beta]^T$ is

$$\hat{\boldsymbol{\vartheta}} = \boldsymbol{\mu} + \boldsymbol{\Gamma}\boldsymbol{H}^T\left(\mathbf{H}\boldsymbol{\Gamma}\boldsymbol{H}^{\mathbf{T}} + \mathbf{C}\right)^{-1}\left(\boldsymbol{\zeta} - \mathbf{m}_\zeta(\boldsymbol{\mu})\right) \tag{46}$$

where $\boldsymbol{\mu}$ is the prior mean $\boldsymbol{\mu} = [\theta_\mu\ \ \beta_\mu]^T$. The columns of the matrix $\boldsymbol{H}$ and the diagonal elements of the diagonal

matrix $\boldsymbol{\Gamma}$ are given by the following:

$$\begin{cases} [\boldsymbol{H}]_{:1} = \beta_\mu^2 \boldsymbol{a} \odot \boldsymbol{a}_{\boldsymbol{\theta}} \odot \left(\boldsymbol{a} \odot \boldsymbol{a} \beta_\mu^2 + \frac{\sigma_d^2}{2} \right)^{\odot \frac{-1}{2}} \\ [\boldsymbol{H}]_{:2} = \beta_\mu \boldsymbol{a} \odot \boldsymbol{a} \odot \left(\boldsymbol{a} \odot \boldsymbol{a} \beta_\mu^2 + \frac{\sigma_d^2}{2} \right)^{\odot \frac{-1}{2}} \\ [\boldsymbol{\Gamma}]_{11} = v^2 \\ [\boldsymbol{\Gamma}]_{22} = \left(\beta_\mu - \beta_v \right)^2 \end{cases} \tag{47}$$

The dependency of $\boldsymbol{a}(\theta_\mu, \boldsymbol{\theta_{BO}})$ and $\boldsymbol{a}_{\boldsymbol{\theta}}(\theta_\mu, \boldsymbol{\theta_{BO}})$ on θ_μ and $\boldsymbol{\theta_{BO}}$ was omitted from (47) for ease of notation. Both θ_μ and v are obtained using (45), and β_μ and β_v are given by the following:

$$\begin{cases} \beta_\mu = \dfrac{\boldsymbol{a}\left(\theta_\mu, \boldsymbol{\theta_{BO}}\right)^T \boldsymbol{\zeta}}{\boldsymbol{a}\left(\theta_\mu, \boldsymbol{\theta_{BO}}\right)^T \boldsymbol{a}\left(\theta_\mu, \boldsymbol{\theta_{BO}}\right)} \\ \beta_v = \dfrac{\boldsymbol{a}\left(\theta_\mu + v, \boldsymbol{\theta_{BO}}\right)^T \boldsymbol{\zeta}}{\boldsymbol{a}\left(\theta_\mu + v, \boldsymbol{\theta_{BO}}\right)^T \boldsymbol{a}\left(\theta_\mu + v, \boldsymbol{\theta_{BO}}\right)} \end{cases} \tag{48}$$

The justification for setting the prior pdf parameters is the same as for the complex amplitude case.

B. The BCRLB

The BCRLB is presented here to determine the performance limit of the MMSE estimator. The BCRLB is given by the following [43]:

$$\begin{cases} BCRLB\left(\left[\hat{\boldsymbol{\vartheta}}\right]_i\right) \geq \left[\boldsymbol{W}\boldsymbol{I}_B^{-1}\boldsymbol{W}\right]_{ii}; \quad i = 1, \ldots K \\ \boldsymbol{W} = \boldsymbol{1} + \dfrac{\partial \boldsymbol{B}\left(\hat{\boldsymbol{\vartheta}}\right)}{\partial \boldsymbol{\vartheta}} + \boldsymbol{B}\left(\hat{\boldsymbol{\vartheta}}\right) \dfrac{\partial \ln p\left(\boldsymbol{\vartheta}\right)}{\partial \boldsymbol{\vartheta}}^T \\ \boldsymbol{I_B} = \boldsymbol{J} + \dfrac{\partial \ln p\left(\boldsymbol{\vartheta}\right)}{\partial \boldsymbol{\vartheta}} \dfrac{\partial \ln p\left(\boldsymbol{\vartheta}\right)}{\partial \boldsymbol{\vartheta}}^T \end{cases} \tag{49}$$

1) *Complex Amplitude Case*: The bias $\boldsymbol{B}(\hat{\boldsymbol{\vartheta}}) = E\{\hat{\boldsymbol{\vartheta}}\} - \boldsymbol{\vartheta}$ of the MMSE estimator is given by the following:

$$\boldsymbol{B}(\hat{\boldsymbol{\vartheta}}) = \mathrm{Re}\left\{\boldsymbol{\mu} - \boldsymbol{\vartheta} + \boldsymbol{\Gamma}\boldsymbol{H}^{\boldsymbol{H}}\left(\boldsymbol{H}\boldsymbol{\Gamma}\boldsymbol{H}^{\boldsymbol{H}} + \boldsymbol{R}\right)^{-1}(\boldsymbol{b}\boldsymbol{a} - \boldsymbol{m}_{\boldsymbol{Z}}(\boldsymbol{\mu}))\right\} \tag{50}$$

The dependency of $\boldsymbol{a}(\theta_{ET},\ \boldsymbol{\theta_{BO}})$ on θ_{ET} and $\boldsymbol{\theta_{BO}}$ was omitted from (50) for ease of notation. $E\{\}$ is the expectation operator. The derivative of $\boldsymbol{B}(\hat{\boldsymbol{\vartheta}})$ with respect to $\boldsymbol{\vartheta}$ is given as follows:

$$\begin{cases} \dfrac{\partial \boldsymbol{B}\left(\hat{\boldsymbol{\vartheta}}\right)}{\partial [\boldsymbol{\vartheta}]_1} \\ = \mathrm{Re}\left\{[-1 \quad 0 \quad 0]^T + \boldsymbol{\Gamma}\boldsymbol{H}^{\boldsymbol{H}}\left(\boldsymbol{H}\boldsymbol{\Gamma}\boldsymbol{H}^{\boldsymbol{H}} + \boldsymbol{R}\right)^{-1}(\boldsymbol{b}\boldsymbol{a}_\theta)\right\} \\ \dfrac{\partial \boldsymbol{B}\left(\hat{\boldsymbol{\vartheta}}\right)}{\partial [\boldsymbol{\vartheta}]_2} \\ = \mathrm{Re}\left\{[0 \quad -1 \quad 0]^T + \boldsymbol{\Gamma}\boldsymbol{H}^{\boldsymbol{H}}\left(\boldsymbol{H}\boldsymbol{\Gamma}\boldsymbol{H}^{\boldsymbol{H}} + \boldsymbol{R}\right)^{-1}(\boldsymbol{a})\right\} \\ \dfrac{\partial \boldsymbol{B}\left(\hat{\boldsymbol{\vartheta}}\right)}{\partial [\boldsymbol{\vartheta}]_3} \\ = \mathrm{Re}\left\{[0 \quad 0 \quad -1]^T + \boldsymbol{\Gamma}\boldsymbol{H}^{\boldsymbol{H}}\left(\boldsymbol{H}\boldsymbol{\Gamma}\boldsymbol{H}^{\boldsymbol{H}} + \boldsymbol{R}\right)^{-1}(j\boldsymbol{a})\right\} \end{cases} \tag{51}$$

The dependency of $\boldsymbol{a}(\theta_{ET}, \boldsymbol{\theta_{BO}})$ and $\boldsymbol{a}_{\boldsymbol{\theta}}(\theta_{ET}, \boldsymbol{\theta_{BO}})$ on θ_{ET} and $\boldsymbol{\theta_{BO}}$ was omitted from (51) for ease of notation. The derivative of the prior pdf natural logarithm is as follows:

$$\begin{cases} \dfrac{\partial \ln p\left(\boldsymbol{\vartheta}\right)}{\partial [\boldsymbol{\vartheta}]_1} = \dfrac{\theta_\mu - \theta_{ET}}{[\boldsymbol{\Gamma}]_{11}} \\ \dfrac{\partial \ln p\left(\boldsymbol{\vartheta}\right)}{\partial [\boldsymbol{\vartheta}]_2} = \dfrac{b_{\mu R} - b_R}{[\boldsymbol{\Gamma}]_{22}} \\ \dfrac{\partial \ln p\left(\boldsymbol{\vartheta}\right)}{\partial [\boldsymbol{\vartheta}]_3} = \dfrac{b_{\mu I} - b_I}{[\boldsymbol{\Gamma}]_{33}} \end{cases} \tag{52}$$

The matrices $\boldsymbol{H}$ and $\boldsymbol{\Gamma}$ are obtained using (44), and the prior Gaussian pdf parameters are given by the following:

$$\begin{cases} \theta_\mu = [\boldsymbol{\theta_{BO}}]_1 + \dfrac{[\boldsymbol{\theta_{BO}}]_N - [\boldsymbol{\theta_{BO}}]_1}{2} \\ v = \dfrac{1}{2}\left(\theta_{um} - ([\boldsymbol{\theta_{BO}}]_N - [\boldsymbol{\theta_{BO}}]_1)\right) \\ b_{\mu R} = \mathrm{Re}\left\{\dfrac{\boldsymbol{a}\left(\theta_\mu, \boldsymbol{\theta_{BO}}\right)^{\boldsymbol{H}} \boldsymbol{R}^{-1} b\boldsymbol{a}\left(\theta_{ET}, \boldsymbol{\theta_{BO}}\right)}{\boldsymbol{a}\left(\theta_\mu, \boldsymbol{\theta_{BO}}\right)^{\boldsymbol{H}} \boldsymbol{R}^{-1} \boldsymbol{a}\left(\theta_\mu, \boldsymbol{\theta_{BO}}\right)}\right\} \\ b_{\mu I} = \mathrm{Im}\left\{\dfrac{\boldsymbol{a}\left(\theta_\mu, \boldsymbol{\theta_{BO}}\right)^{\boldsymbol{H}} \boldsymbol{R}^{-1} b\boldsymbol{a}\left(\theta_{ET}, \boldsymbol{\theta_{BO}}\right)}{\boldsymbol{a}\left(\theta_\mu, \boldsymbol{\theta_{BO}}\right)^{\boldsymbol{H}} \boldsymbol{R}^{-1} \boldsymbol{a}\left(\theta_\mu, \boldsymbol{\theta_{BO}}\right)}\right\} \\ b_{vR} = \mathrm{Re}\left\{\dfrac{\boldsymbol{a}\left(\theta_\mu + v, \boldsymbol{\theta_{BO}}\right)^{\boldsymbol{H}} \boldsymbol{R}^{-1} b\boldsymbol{a}\left(\theta_{ET}, \boldsymbol{\theta_{BO}}\right)}{\boldsymbol{a}\left(\theta_\mu + v, \boldsymbol{\theta_{BO}}\right)^{\boldsymbol{H}} \boldsymbol{R}^{-1} \boldsymbol{a}\left(\theta_\mu + v, \boldsymbol{\theta_{BO}}\right)}\right\} \\ b_{vI} = \mathrm{Im}\left\{\dfrac{\boldsymbol{a}\left(\theta_\mu + v, \boldsymbol{\theta_{BO}}\right)^{\boldsymbol{H}} \boldsymbol{R}^{-1} b\boldsymbol{a}\left(\theta_{ET}, \boldsymbol{\theta_{BO}}\right)}{\boldsymbol{a}\left(\theta_\mu + v, \boldsymbol{\theta_{BO}}\right)^{\boldsymbol{H}} \boldsymbol{R}^{-1} \boldsymbol{a}\left(\theta_\mu + v, \boldsymbol{\theta_{BO}}\right)}\right\} \end{cases} \tag{53}$$

2) *Amplitude Case*: The bias $\boldsymbol{B}(\hat{\boldsymbol{\vartheta}}) = E\{\hat{\boldsymbol{\vartheta}}\} - \boldsymbol{\vartheta}$ of the MMSE estimator is given by the following:

$$\begin{aligned} \boldsymbol{B}\left(\hat{\boldsymbol{\vartheta}}\right) = \boldsymbol{\mu} - \boldsymbol{\vartheta} + \boldsymbol{\Gamma}\boldsymbol{H}^T\left(\boldsymbol{H}\boldsymbol{\Gamma}\boldsymbol{H}^T + \boldsymbol{C}\right)^{-1} \\ \times \left(\left(\boldsymbol{a} \odot \boldsymbol{a}\beta^2 + \frac{\sigma_d^2}{2}\right)^{\odot \frac{1}{2}} - \mathbf{m}_\zeta(\boldsymbol{\mu})\right) \end{aligned} \tag{54}$$

The dependency of $\boldsymbol{a}(\theta_{ET}, \boldsymbol{\theta_{BO}})$ on θ_{ET} and $\boldsymbol{\theta_{BO}}$ was omitted from (54) for ease of notation. The derivative of $\boldsymbol{B}(\hat{\boldsymbol{\vartheta}})$ with respect to $\boldsymbol{\vartheta}$ is given as follows:

$$\begin{cases} \dfrac{\partial \boldsymbol{B}\left(\hat{\boldsymbol{\vartheta}}\right)}{\partial [\boldsymbol{\vartheta}]_1} = [-1 \quad 0]^T + \boldsymbol{\Gamma}\boldsymbol{H}^T\left(\boldsymbol{H}\boldsymbol{\Gamma}\boldsymbol{H}^T + \boldsymbol{C}\right)^{-1} \\ \qquad \left(\beta^2 \boldsymbol{a} \odot \boldsymbol{a}_\theta \odot \left(\boldsymbol{a} \odot \boldsymbol{a}\beta^2 + \dfrac{\sigma_d^2}{2}\right)^{\odot \frac{-1}{2}}\right) \\ \dfrac{\partial \boldsymbol{B}\left(\hat{\boldsymbol{\vartheta}}\right)}{\partial [\boldsymbol{\vartheta}]_2} = [0 \quad -1]^T + \Gamma\boldsymbol{H}^T\left(\boldsymbol{H}\boldsymbol{\Gamma}\boldsymbol{H}^T + \boldsymbol{C}\right)^{-1} \\ \qquad \left(\beta \boldsymbol{a} \odot \boldsymbol{a} \odot \left(\boldsymbol{a} \odot \boldsymbol{a}\beta^2 + \dfrac{\sigma_d^2}{2}\right)^{\odot \frac{-1}{2}}\right) \end{cases} \tag{55}$$

The dependency of $\boldsymbol{a}(\theta_{ET},\ \boldsymbol{\theta_{BO}})$ and $\boldsymbol{a}_{\boldsymbol{\theta}}(\theta_{ET}, \boldsymbol{\theta_{BO}})$ on θ_{ET} and $\boldsymbol{\theta_{BO}}$ was omitted from (55) for ease of notation. The

TABLE IV
Simulation Setups Used to Evaluate Performance of Estimators[1]

Setup	$\theta_B = \theta_{um}$	θ_{ET}	N	$PRI\omega_R$	$[\boldsymbol{\theta_{BO}}]_1$	$[\boldsymbol{\theta_{BO}}]_N$
1	30°	15°	32	0.9375°	0°	29.0625°
2	30°	15°	16	1.2667°	0°	19°
3	30°	15°	8	3.2857°	0°	23°

Parameters listed are spinning antenna beamwidth θ_B, unambiguous width θ_{um}, emitter DOA θ_{ET}, number of pulses N, the product of the pulse repetition interval and angular velocity ($PRI\omega_R$), and antenna boresight angle vector $\boldsymbol{\theta_{BO}}$.

derivative of the prior pdf natural logarithm is as follows:

$$\begin{cases} \dfrac{\partial \ln p(\boldsymbol{\vartheta})}{\partial[\boldsymbol{\vartheta}]_1} = \dfrac{\theta_\mu - \theta_{ET}}{[\boldsymbol{\Gamma}]_{11}} \\ \dfrac{\partial \ln p(\boldsymbol{\vartheta})}{\partial[\boldsymbol{\vartheta}]_2} = \dfrac{\beta_\mu - \beta}{[\boldsymbol{\Gamma}]_{22}} \end{cases} \tag{56}$$

The matrices $\boldsymbol{H}$ and $\boldsymbol{\Gamma}$ are obtained using (47), θ_μ and v are obtained using (53), and β_μ and β_v are given by the following:

$$\begin{cases} \beta_\mu = \dfrac{\boldsymbol{a}\left(\theta_\mu, \boldsymbol{\theta_{BO}}\right)^T \left(\boldsymbol{a} \odot \boldsymbol{a}\beta^2 + \dfrac{\sigma_d^2}{2}\right)^{\odot\frac{1}{2}}}{\boldsymbol{a}\left(\theta_\mu, \boldsymbol{\theta_{BO}}\right)^T \boldsymbol{a}\left(\theta_\mu, \boldsymbol{\theta_{BO}}\right)} \\ \beta_v = \dfrac{\boldsymbol{a}\left(\theta_\mu + v, \boldsymbol{\theta_{BO}}\right)^T \left(\boldsymbol{a} \odot \boldsymbol{a}\beta^2 + \dfrac{\sigma_d^2}{2}\right)^{\odot\frac{1}{2}}}{\boldsymbol{a}\left(\theta_\mu + v, \boldsymbol{\theta_{BO}}\right)^T \boldsymbol{a}\left(\theta_\mu + v, \boldsymbol{\theta_{BO}}\right)} \end{cases} \tag{57}$$

The dependency of $\boldsymbol{a}(\theta_{ET}, \boldsymbol{\theta_{BO}})$ on θ_{ET} and $\boldsymbol{\theta_{BO}}$ was omitted from (57) for ease of notation.

VII. PERFORMANCE ANALYSIS

The performance of the proposed estimators was investigated by means of a Monte Carlo simulation in terms of the MSE and compared to the unbiased estimation bounds and the BCRLB. The MSE is defined as follows:

$$MSE = E\left\{\left(\hat{\theta}_{ET} - \theta_{ET}\right)^2\right\} \tag{58}$$

The simulations were performed with a Gaussian beam shape for the spinning antenna and assuming ideal detection and amplitude measurement by the digital receiver. The DOA θ_{ET}, the complex amplitude b, and the amplitude β are deterministic unknowns, while the disturbance $\boldsymbol{d}$ is composed of complex white Gaussian noise with zero mean and a known covariance matrix. The simulation scenarios illustrated in Table IV were performed, where simulation setups 2 and 3 represent the partial spread of pulses across the antenna unambiguous width scenarios:

In Fig. 6, the performance of the ML estimator in (21) is compared to the performance of the ML estimator in (17) for the first simulation setup. Fig. 6 clearly illustrates that the approximation is good. The detailed simulation results are shown in Figs. 7 to 12, which plot the estimation bounds and the MSE, bias, and variance for the different

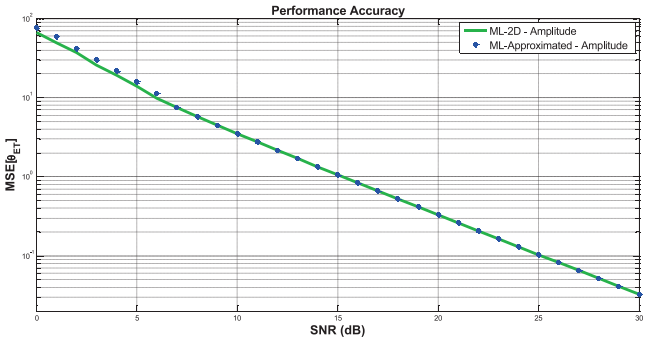

Fig. 6. $MSE\{\hat{\theta}_{ET}\}$ performance of ML-2D estimator versus approximated ML estimator for first simulation setup. $\theta_B = \theta_{um} = 30°$, $\theta_{ET} = 15°$, $N = 32$, $PRI\ \omega_R = 0.9375°$, $[\boldsymbol{\theta_{BO}}]_1 = 0°$, and $[\boldsymbol{\theta_{BO}}]_N = 29.0625°$.

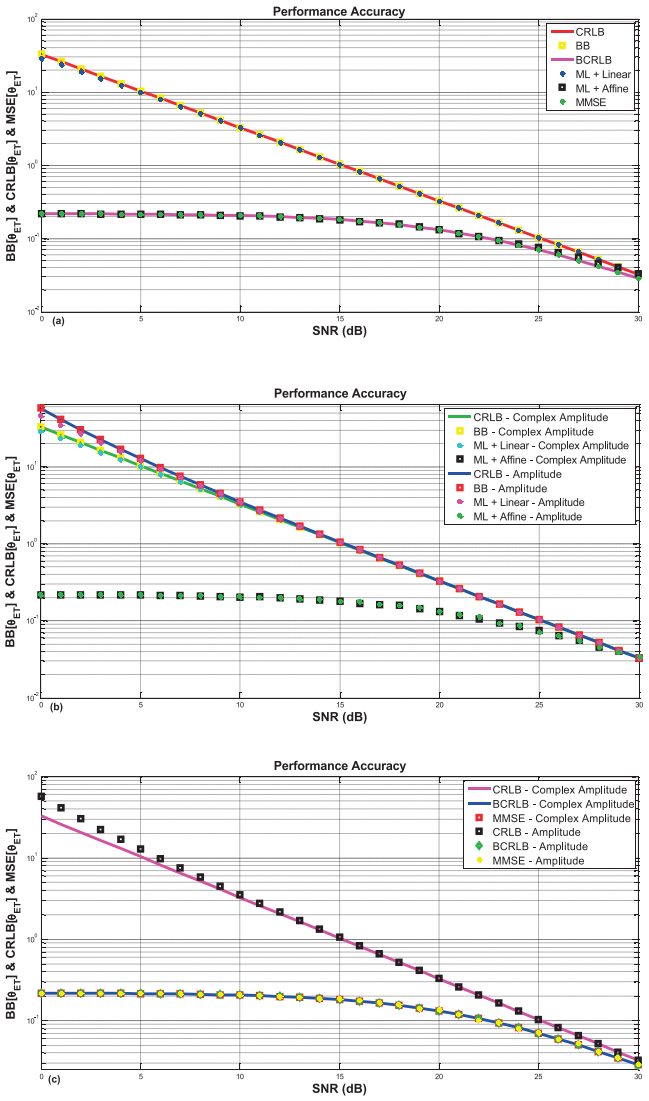

Fig. 7. $MSE\{\hat{\theta}_{ET}\}$ performance of estimators versus estimation bounds for first simulation setup. (a) Transformed ML estimators and MMSE estimator versus estimation bounds for complex amplitude case. (b) Transformed ML estimators for complex amplitude case and amplitude case versus estimation bounds. (c) MMSE estimator for complex amplitude case and amplitude case versus estimation bounds. $\theta_B = \theta_{um} = 30°$, $\theta_{ET} = 15°$, $N = 32$, $PRI\ \omega_R = 0.9375°$, $[\boldsymbol{\theta_{BO}}]_1 = 0°$, and $[\boldsymbol{\theta_{BO}}]_N = 29.0625°$.

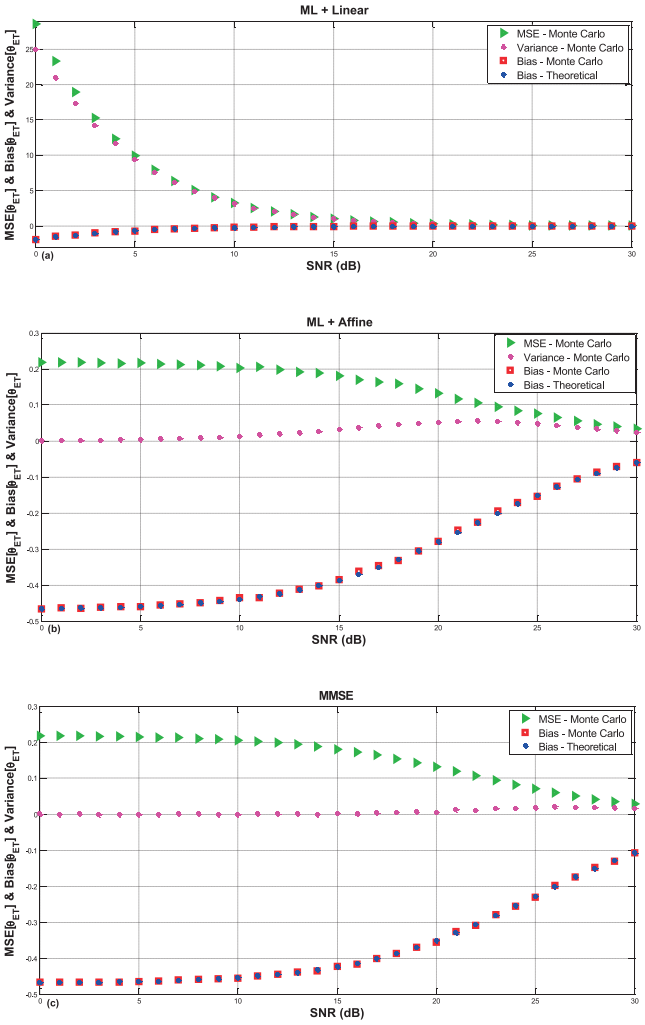

Fig. 8. Bias$\{\hat{\theta}_{ET}\}$, var$\{\hat{\theta}_{ET}\}$, and $MSE\{\hat{\theta}_{ET}\}$ of estimators for first simulation setup. (a) Linearly transformed ML estimator. (b) Affine transformed ML estimator. (c) MMSE estimator. $\theta_B = \theta_{um} = 30°$, $\theta_{ET} = 15°$, $N = 32$, $PRI\ \omega_R = 0.9375°$, $[\boldsymbol{\theta_{BO}}]_1 = 0°$, and $[\boldsymbol{\theta_{BO}}]_N = 29.0625°$.

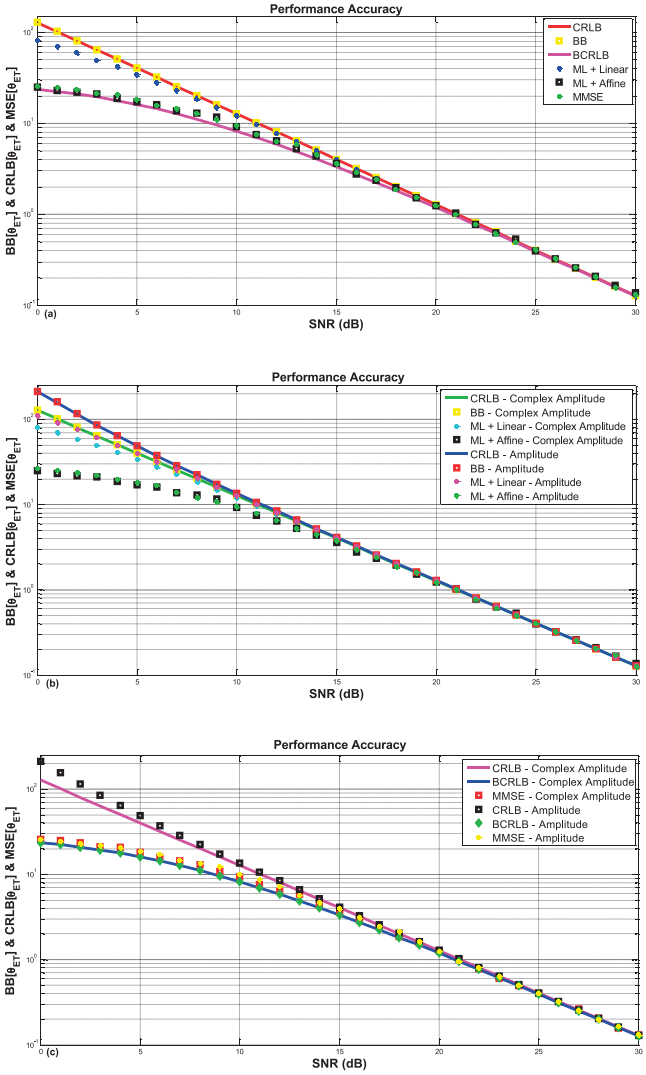

Fig. 9. $MSE\{\hat{\theta}_{ET}\}$ performance of estimators versus estimation bounds for second simulation setup. (a) Transformed ML estimators and MMSE estimator versus estimation bounds for complex amplitude case. (b) Transformed ML estimators for complex amplitude case and amplitude case versus estimation bounds. (c) MMSE estimator for complex amplitude case and amplitude case versus estimation bounds. $\theta_B = \theta_{um} = 30°$, $\theta_{ET} = 15°$, $N = 16$, $PRI\ \omega_R = 1.2667°$, $[\boldsymbol{\theta_{BO}}]_1 = 0°$, and $[\boldsymbol{\theta_{BO}}]_N = 19°$.

estimators versus the SNR. Three MSE performance plots per simulation setup were plotted to avoid cluttering the figures, and only the bias and variance of the estimators that use the complex amplitude were plotted.

In Figs. 7 and 8, the first simulation setup is investigated, which is a full-spread scenario. The improvement in the MSE performance provided by the affine transformed ML estimator and the MMSE estimator is well evident, even when the SNR value is large. The introduced bias dominates the MSE, and the variance converges to zero. In Figs. 9 to 12, the second and third simulation setups are investigated, which are partial-spread scenarios. The affine transformed ML estimator and the MMSE estimator provide excellent improvement in MSE performance, but they are not as significant as in the full-spread scenario. The introduced bias increases as the SNR decreases, dominating the MSE and forcing the variance to decrease.

The numerical results obtained show that the DOA estimators did not experience the threshold effect even for low values of N and SNR. These results are in agreement with the BB not deviating from the CRLB. Moreover, the numerical results show that the proposed biased estimators outperform the unbiased estimation bounds for all possible scenarios and that the MMSE estimator performance is close to that of the BCRLB. The simulation results also show that the affine transformed ML estimator and the MMSE estimator provide the best performance for low number of pulses and/or low SNR. Moreover, the performance of the biased estimators is similar for both cases (the complex amplitude case and the amplitude case) because the MSE is dominated by the bias component when the number of pulses is low and/or the SNR is low. When compared to the affine transformed ML estimator, the MMSE estimator does not require the computation

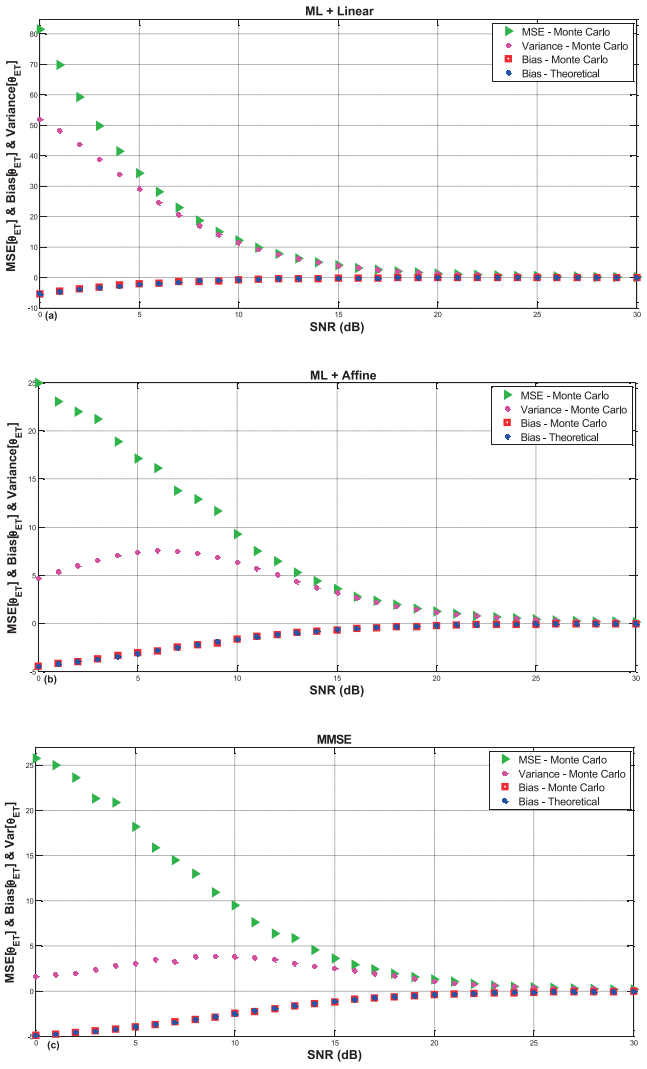

Fig. 10. Bias$\{\hat{\theta}_{ET}\}$, var$\{\hat{\theta}_{ET}\}$, and $MSE\{\hat{\theta}_{ET}\}$ of estimators for second simulation setup. (a) Linearly transformed ML estimator. (b) Affine transformed ML estimator. (c) MMSE estimator. $\theta_B = \theta_{um} = 30°$, $\theta_{ET} = 15°$, $N = 16$, $PRI\ \omega_R = 1.2667°$, $[\boldsymbol{\theta_{BO}}]_1 = 0°$, and $[\boldsymbol{\theta_{BO}}]_N = 19°$.

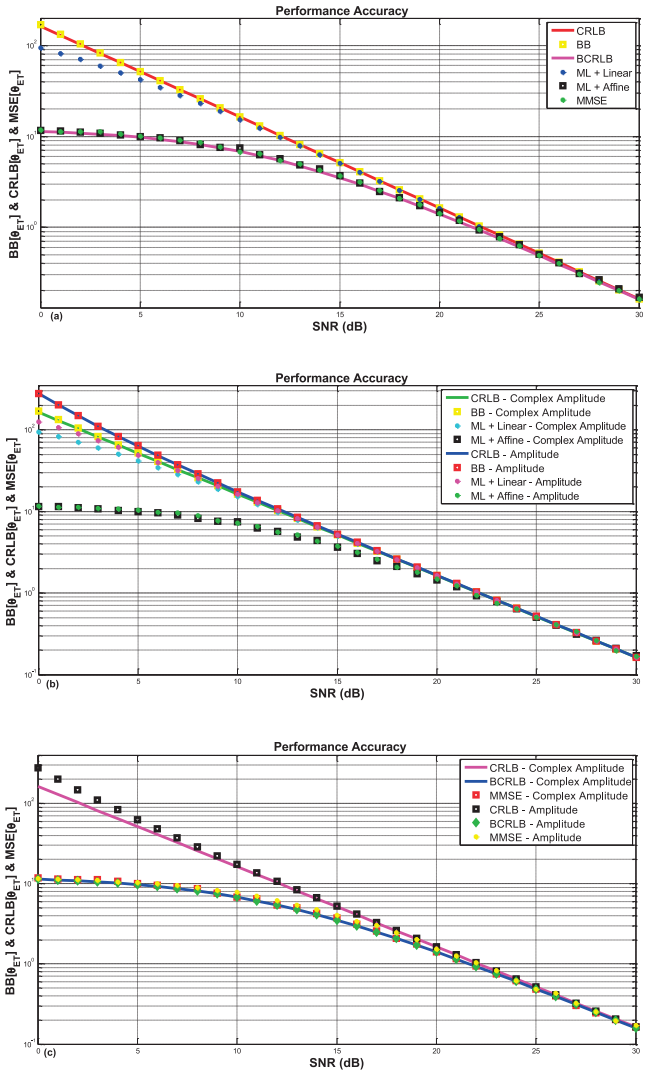

Fig. 11. $MSE\{\hat{\theta}_{ET}\}$ performance of estimators versus estimation bounds for third simulation setup. (a) Transformed ML estimators and MMSE estimator versus estimation bounds for complex amplitude case. (b) Transformed ML estimators for complex amplitude case and amplitude case versus estimation bounds. (c) MMSE estimator for complex amplitude case and amplitude case versus estimation bounds. $\theta_B = \theta_{um} = 30°$, $\theta_{ET} = 15°$, $N = 8$, $PRI\ \omega_R = 3.2857°$, $[\boldsymbol{\theta_{BO}}]_1 = 0°$, and $[\boldsymbol{\theta_{BO}}]_N = 23°$.

over a predefined grid; thus, the MMSE estimator has less computational load and is easier to implement.

It was found that the optimal values of m and u returned by (29), (36), and (37) always conform to the optimal values of m and u for $\theta = [\boldsymbol{\theta_{BO}}]_1 + \theta_{um}/2$, provided that the antenna mainlobe is symmetrical around its peak. This means that m for the linearly transformed ML estimator can be found directly by using (32):

$$m = -\frac{CRLB}{CRLB + \left([\boldsymbol{\theta_{BO}}]_1 + \dfrac{\theta_{um}}{2}\right)^2} \tag{59}$$

It also means that m and u for the affine transformed ML estimator can be found directly by using (40) and (41):

$$\begin{cases} m = -\dfrac{CRLB}{CRLB + b_1^T b_1 - c_1} \\ u = -\dfrac{CRLB}{CRLB + b_1^T b_1 - c_1} b_1 \end{cases} \tag{60}$$

The dependency of $CRLB([\boldsymbol{\theta_{BO}}]_1 + \theta_{um}/2)$ on $[\boldsymbol{\theta_{BO}}]_1 + \theta_{um}/2$ was omitted from (59) and (60) for ease of notation. Other simulation scenarios with different parameter values were also performed, and the conclusions obtained remain the same.

VIII. EXPERIMENTAL RESULTS

The proposed estimators were applied to real data provided by Reutech Radar Systems [50]. The experiment was realized by using a mechanically scanning L-band

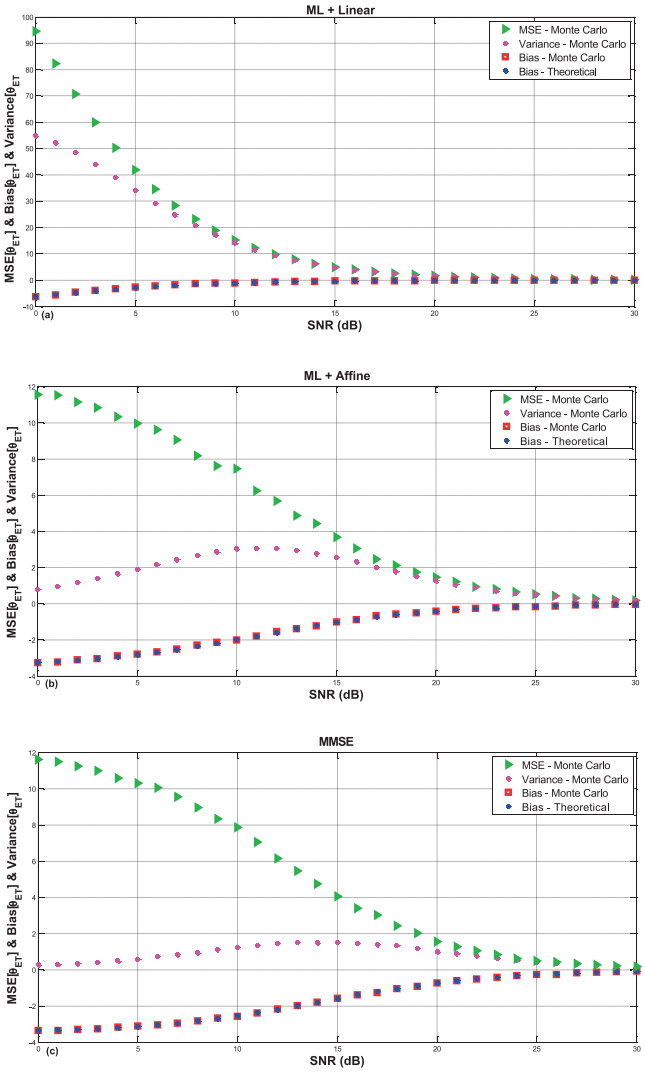

Fig. 12. Bias$\{\hat{\theta}_{ET}\}$, var$\{\hat{\theta}_{ET}\}$, and $MSE\{\hat{\theta}_{ET}\}$ of estimators for third simulation setup. (a) Linearly transformed ML estimator. (b) Affine transformed ML estimator. (c) MMSE estimator. $\theta_B = \theta_{um} = 30°$, $\theta_{ET} = 15°$, $N = 8$, PRI $\omega_R = 3.2857°$, $[\theta_{BO}]_1 = 0°$, and $[\boldsymbol{\theta_{BO}}]_N = 23°$.

radar and a transponder beacon placed 10 km away from the radar. The radar transmits a waveform, and then the transponder beacon retransmits the radar waveform when illuminated by the radar. The waveform is sequentially frequency diverse across three frequencies, with 32 pulses for each frequency at 4 kHz of pulse repetition frequency. The rotation rate of the radar antenna is 30 rpm, and the beamwidth is 7.3°. The radar waveform is modulated by the two-way radar antenna beam pattern, and the antenna mainlobe is fitted to a Gaussian model.

The recorded data are shown in Fig. 13, where each frequency is highlighted by a different color. The red patch that is pointed at in the figure is used for DOA estimation to emulate an extreme case of a partial-spread scenario. The measured SNR is 15 dB. Synthesized white Gaussian noise was injected into the recorded data to obtain different values of the SNR. The MSE, bias and variance of the estimators are shown in Figs. 14 and 15. Fig. 14 clearly shows that the MMSE estimator and the affine transformed ML

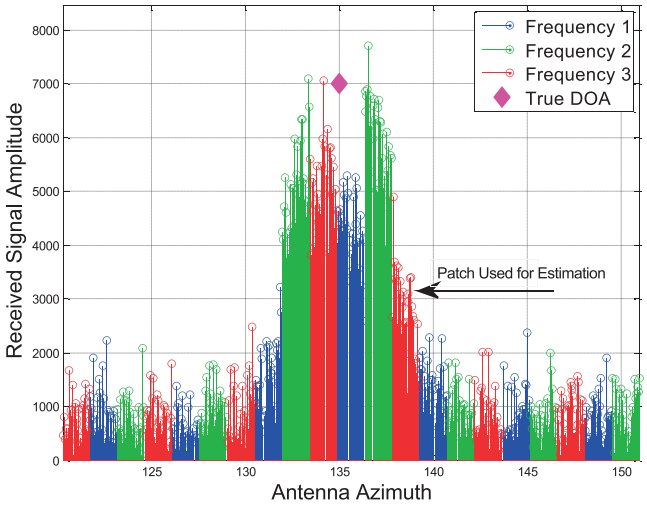

Fig. 13. Data recorded using L-band radar and transponder beacon. $\theta_B = \theta_{um} = 7.3°$, $\theta_{ET} = 134.9582°$, $N = 32$, $[\boldsymbol{\theta_{BO}}]_1 = 137.8015°$, and $[\boldsymbol{\theta_{BO}}]_N = 139.2188°$.

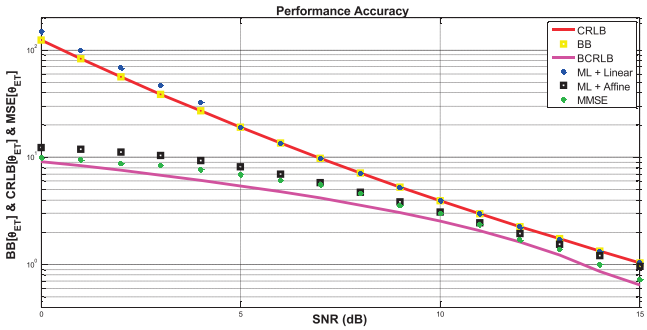

Fig. 14. $MSE\{\hat{\theta}_{ET}\}$ performance of estimators versus estimation bounds for data recorded using L-band radar and transponder beacon. $\theta_B = \theta_{um} = 7.3°$, $\theta_{ET} = 134.9582°$, $N = 32$, $[\boldsymbol{\theta_{BO}}]_1 = 137.8015°$, and $[\boldsymbol{\theta_{BO}}]_N = 139.2188°$.

estimator significantly outperform the unbiased estimation bounds and that the MMSE estimator performance is close to that of the BCRLB. There is no significant bias introduced to the linearly transformed ML estimator because of the large value of the azimuth angle, while the slight deviation from the CRLB is because of mismatch caused by the approximation of the ML estimator.

IX. CONCLUSION

In this work, biased DOA estimators of emitters present in the spinning antenna mainlobe of an ELINT system were proposed. These estimators were constructed by using Bayesian estimation techniques and by performing a linear transformation and an affine transformation on the ML estimator. The performance of the proposed estimators was investigated by means of experimental studies and a Monte Carlo simulation as a function of the SNR, the DOA, the number of pulses, and the spread of pulses across the antenna unambiguous width. We found that the proposed estimators outperformed the performance limit set by the unbiased estimation bounds and that the MMSE estimator

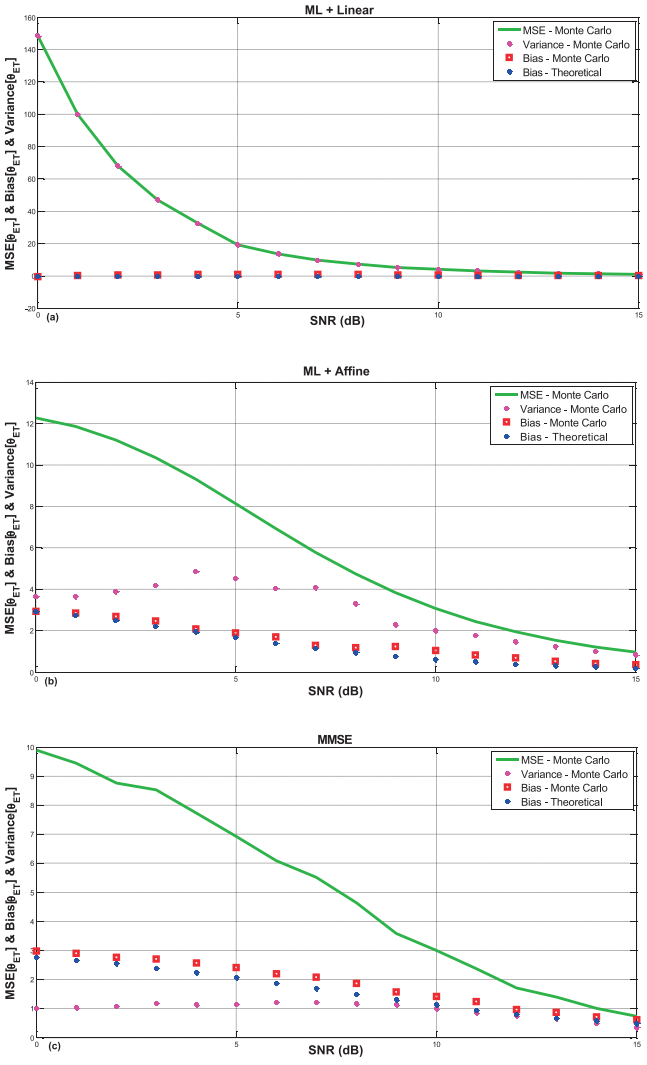

Fig. 15. Bias$\{\hat{\theta}_{ET}\}$, var$\{\hat{\theta}_{ET}\}$, and $MSE\{\hat{\theta}_{ET}\}$ of estimators for data recorded using L-band radar and transponder beacon. (a) Linearly transformed ML estimator. (b) Affine transformed ML estimator. (c) MMSE estimator. $\theta_B = \theta_{um} = 7.3°$, $\theta_{ET} = 134.9582°$, $N = 32$, $[\boldsymbol{\theta_{BO}}]_1 = 137.8015°$, and $[\boldsymbol{\theta_{BO}}]_N = 139.2188°$.

performance is close to that of the BCRLB. In addition, we found that the affine transformed ML estimator and the MMSE estimator performed adequately for the possible scenarios that spinning antenna-based ELINT systems might encounter, i.e., when the antenna beamwidth is wide, when the number of pulses is low and/or the SNR is low, or when the intercepted pulses are partially spread across the antenna unambiguous width.

This work can be extended to the field of radar, similar to [1, 2], and to investigation of the performance of the biased estimators when b is modeled as Gaussian distributed random complex amplitude.

ACKNOWLEDGMENT

We are grateful to King Abdulaziz City for Science and Technology for the financial support received to carry out this work.

FUAD ALIBRAHIM
MICHAEL INGGS
Department of Electrical Engineering
University of Cape Town
Private Bag, Rondebosch
Cape Town, 7701 South Africa
E-mail: (fibrahiem@kacst.edu.sa)

REFERENCES

[1] Farina, A., Gini, F., and Greco, M.
DOA Estimation by exploiting the amplitude modulation induced by antenna scanning.
IEEE Transactions on Aerospace and Electronic Systems, **38** (Oct. 2002), 1276–1286.

[2] Gini, F., Greco, M., and Farina, A.
Multiple radar targets estimation by exploiting induced amplitude modulation.
IEEE Transactions on Aerospace and Electronic Systems, **39** (Oct. 2003), 1316–1332.

[3] Greco, M., Gini, F., Farina, A., and Timmoneri, L.
Direction-of-arrival estimation in radar systems: Moving window against approximate maximum likelihood estimator.
IET Radar, Sonar and Navigation, **3**, 5 (2009), 552–557.

[4] Zhang, S., Wan, Q., and Wang, H.
DOA estimation in mechanical scanning radar systems using sparse signal reconstruction methods.
In *Proceedings of the WICOM Conference*, 2011, 1–4.

[5] Farina, A., Gabatel, G., and Sanzullo, R.
Estimation of target direction by pseudo-monopulse algorithm.
Signal Processing, **80** (2000), 295–310.

[6] Galati, G., and Studer, F.
Maximum likelihood azimuth estimation applied to SSR/IFF systems.
IEEE Transactions on Aerospace and Electronic Systems, **26** (1990), 27–43.

[7] Swerling, P.
Maximum angular accuracy of a pulsed search radar.
Proceedings of the IRE, **44** (Sept. 1956), 1146–1155.

[8] Efron, B.
Biased versus unbiased estimation.
Advanced Mathematics, **16** (1975), 259–277.

[9] Kay, S., and Eldar, Y.
Rethinking biased estimation [lecture notes].
IEEE Signal Processing Magazine, **25** (May 2008), 133–136.

[10] Eldar, Y.
Uniformly improving the Cramer-Rao bound and maximum-likelihood estimation.
IEEE Transactions on Signal Processing, **54** (Aug. 2006), 2934–2956.

[11] Eldar, Y.
MSE bounds with affine bias dominating the Cramer-Rao bound.
IEEE Transactions on Signal Processing, **56** (Aug. 2008), 3824–3836.

[12] Eldar, Y.
Rethinking biased estimation: Improving maximum likelihood and the Cramer-Rao bound.
Foundations and Trends in Signal Processing, **1**, 4 (2007), 305–449.

[13] De Martino, A.
Introduction to Modern EW Systems (Radar). Norwood, MA: Artech House, 2012.

[14] Kay, S.
Fundamentals of Statistical Signal Processing, Estimation Theory. Englewood Cliffs, NJ: Prentice Hall, 1993.

[15] Tsui, J.
Digital Techniques for Wideband Receivers. Raleigh, NC: SciTech Publishing, 2004.

[16] Lipsky, E.
Microwave Passive Direction Finding. Raleigh, NC: SciTech Publishing, 2004, p. 15.

[17] Naval Air Systems.
Electronic Warfare and Radar Systems Engineering Handbook. Raleigh, NC: Naval Air Systems, ALIAND, 2010.

[18] Stimson, G.
Stimson's Introduction to Airborne Radar. Edison, NJ: SciTech Publishing, 2014.

[19] Adamy, D.
EW 101: A First Course in Electronic Warfare. Norwood, MA: Artech House, 2001, p. 154.

[20] Skolnik, M.
Radar Handbook (3rd ed.). New York, NY: McGraw-Hill, 2008.

[21] Optimization interface (OPTI) toolbox OPTI toolbox wiki, http://www.i2c2.aut.ac.nz/Wiki/OPTI/.

[22] Rockwell Collins ANT-1040A airborne spinning antenna, http://www.rockwellcollins.com/sitecore/content/Data/Products/EW_and_Intelligence/SIGINT/ANT-1040A_Airborne_Spinning_DF_Antenna.aspx.

[23] Rockwell Collins Signals intelligence antennas, http://www.rockwellcollins.com/Products_and_Systems/EW_and_Intelligence/SIGINT.aspx.

[24] ASC Signal Direction finding antennas. Available: http://ascsignal.com/other/direction-finding-antennas/.

[25] Antenna Research Integrated antenna systems. Available: http://emc.vwh.net/PDF-RF/094-096.pdf.

[26] Microwave Technologies Group Microwave Technologies Group catalogue. Available: http://www.mtginc.co.kr/support/total%20catalogue_100426.pdf.

[27] Akhdar, O., Carsenat, D., Decroze, C., and Monediere, T.
A simple technique for angle of arrival measurement.
In *Proceedings of the Antenna and Propagation Society International Symposium (AP-S)*, 2008, 1–4.

[28] Akhdar, O., Carsenat, D., Decroze, C., and Mouhamadou, M.
A new CLEAN algorithm for angle of arrival denoising.
IEEE Antennas and Wireless Propagation Letters, **8** (2009), 478–481.

[29] Lie, J., Blu, T., and See, C.
Single antenna power measurements based direction finding.
IEEE Transactions Signal Processing, **58**, 11 (2010), 5682–5692.

[30] Lie, J., Blu, T., and See, C.
Single antenna power measurements based direction finding with incomplete spatial coverage.
In *Proceedings of the IEEE International Conference on Acoustics, Speech and Signal Processing (ICASSP)*, 2012, 2641–2644.

[31] Du Plessis, W., Potgieter, P., Gouws, M., and Malan, E.
Initial results for compressive sensing in electronic support receiver systems.
In *Proceedings of the Electronics, Communications and Photonics Conference (SIECPC)*, 2011, 1–6.

[32] Schultz, H.
Digital receiver experiment or reality.
Presented at the *AOC Aardvark Roost Conference*, Pretoria, South Africa, 2008.

[33] Stoica, P., and Moses, R.
Introduction to Spectral Analysis. Englewood Cliffs, NJ: Prentice Hall, 1997, p. 271.

[34] Zhang, Y., Zhang, Y., Huang, Y., Yang, J., Zha, Y., Wu, J., and Yang, H.
ML iterative superresolution approach for real-beam radar.
In *Proceedings of the IEEE Radar Conference*, 2014, 1192–1196.

[35] Zhang, Y., Xia, Y., Li, W., Huang, Y., and Yang, J.
An improved MUSIC algorithm for angular superresolution in scanning antenna.
In *Proceedings of the International Conference on Computational Problem Solving*, 2013, 358–361.

[36] Shikhar, U., and Goodman, N.
Superresolution of coherent sources in real beam data.
IEEE Transactions on Aerospace and Electronic Systems, **46**, 3, (2010), 1557–1566.

[37] Zha, Y., Huang, Y., Yang, J., Wu, J., and Yang, H.
An improved Richardson-Lucy algorithm for radar angular super-resolution.
In *Proceedings of the IEEE Radar Conference*, 2014, 406–410.

[38] Zhang, Y., Zhang, Y., Huang, Y., Li, W., Zha, Y., and Yang, J.
Angular superresolution for real beam radar with iterative adaptive approach.
In *Proceedings of the IEEE International Geoscience and Remote Sensing Symposium*, 2013, 3100–3103.

[39] Guan, J., Huang, Y., Li, W., and Yang, J.
Maximum a posterior estimation based angular superresolution for scanning radar imaging.
IEEE Transactions on Aerospace and Electronic Systems, **50**, 3 (2014), 2389–2398.

[40] Zhang, Y., Huang, Y., Zha, Y., Wang, Y., and Yang, J.
Real-beam scanning radar angular super-resolution via sparse deconvolution.
In *Proceedings of the IEEE International Geoscience and Remote Sensing Symposium*, 2014, 3081–3084.

[41] Zhang, Y., Zha, Y., Wu, J., Huang, Y., and Yang, J.
Weighted least squares method for forward looking imaging of scanning radar.
In *Proceedings of the IEEE International Geoscience and Remote Sensing Symposium*, 2014, 714–716.

[42] Guan, J., Huang, Y., Li, W., and Yang, J.
Angular super-resolution algorithm based on maximum entropy for scanning radar imaging.
In *Proceedings of the IEEE International Geoscience and Remote Sensing Symposium*, 2014, 3057–3060.

[43] Huang, Y., and Zhang, J.
Lower bounds on the variance of deterministic signal parameter estimators using Bayesian inference.
In *Proceedings of the IEEE International Conference on Acoustics, Speech, and Signal Processing (ICASSP)*, 2003, Vol. 6, 745–748.

[44] Forster, P., and Larzabal, P.
On lower bounds for deterministic parameter estimation.
In *Proceedings of the IEEE International Conference on Acoustics, Speech, and Signal Processing Proceedings. (ICASSP)*, 2003, Vol. 2, 1137–1140.

[45] Tabrikian, J., and Krolik, J.
Barankin bounds for source localization in an uncertain ocean environment.
IEEE Transactions on Signal Processing, **54** (Nov. 1999), 2917–2927.

[46] Adamy, D.
EW 104: Electronic Warfare Against a New Generation of Threats. Norwood, MA: Artech House, 2015.

[47] Association of Old Crows EW/SIGINT online resource guide, http://www.ewsigint.net/.

[48] Thales Group Meerkat-S: High mobility radar band ESM and ELINT system, https://www.thalesgroup.com/en/worldwide/defence/land-forces/vehicles/electronic-warfare/meerkat-s-high-mobility-radar-band-esm-elint-system.

[49] Exelis ES-5080: Wideband digital receiver based ELINT/ESM systems, http://www.exelisinc.com/solutions/ES-5080/Pages/default.aspx.

[50] Reutech Radar Systems, http://www.rrs.co.za/.